AJHG The American Journal of Human Genetics

A syndromic neurodevelopmental disorder caused by rare variants in PPFIA3

--Manuscript Draft--

Manuscript Number:	AJHG-D-23-00227R4
Full Title:	A syndromic neurodevelopmental disorder caused by rare variants in PPFIA3
Article Type:	Article
Keywords:	Neurodevelopmental disorder; Synaptic protein; Active zone protein; Mendelian phenotypes; Fruit flies
Corresponding Author:	Hsiao-Tuan Chao, M.D., Ph.D. Baylor College of Medicine Houston, TX UNITED STATES
First Author:	Maimuna S. Paul
Order of Authors:	Maimuna S. Paul
	Sydney L. Michener
	Hongling Pan
	Hiuling Chan
	Jessica M. Pfliger
	Jill A. Rosenfeld
	Vanesa C. Lerma
	Alyssa Tran
	Megan A. Longley
	Richard A. Lewis
	Monika Weisz-Hubshman
	Mir Reza Bekheirnia
	Nasim Bekheirnia
	Lauren Massingham
	Michael Zech
	Matias Wagner
	Hartmut Engels
	Kirsten Cremer
	Elisabeth Mangold
	Sophia Peters
	Jessica Trautmann
	Jessica L. Mester
	Maria J. Guillen
	Richard Person
	Pamela P. McDonnell
	Stacey R. Cohen
	Laina Lusk
	Ana S.A. Cohen

Jean-Baptiste Le Pichon
Tomi Pastinen
Dihong Zhou
Kendra Engleman
Caroline Racine
Laurence Faivre
Sébastien Moutton
Anne-Sophie Denommé-Pichon
Hyun Yong Koh
Annapurna Poduri
Jeffrey Bolton
Cordula Knopp
Dong Sun Julia Suh
Andrea Maier
Mehran B. Toosi
Ehsan G. Karimiani
Reza Maroofian
Gerald B. Schaefer
Vijayalakshmi Ramakumaran
Pradeep Vasudevan
Chitra Prasad
Matthew Osmond
Sarah Schuhmann
Georgia Vasileiou
Sophie Russ-Hall
Ingrid E. Scheffer
Gemma L. Carvill
Heather Mefford
Carlos A. Bacino
Brendan H. Lee
Hsiao-Tuan Chao, M.D., Ph.D.

Abstract:

PPFIA3 encodes the Protein-Tyrosine-Phosphatase, Receptor-Type, F-Polypeptide-Interacting-Protein-Alpha-3 (PPFIA3), which is a member of the LAR-protein-tyrosine phosphatase-interacting-protein (liprin) family involved in synapse formation and function, synaptic vesicle transport, and presynaptic active zone assembly. The protein structure and function are evolutionarily well-conserved, but human diseases related to PPFIA3 dysfunction are not yet reported in OMIM. Here, we report 20 individuals with rare PPFIA3 variants (19 heterozygous and 1 compound heterozygous) presenting with developmental delay, intellectual disability, hypotonia, dysmorphisms, microcephaly or macrocephaly, autistic features, and epilepsy with reduced penetrance. Seventeen unique PPFIA3 variants were detected in 18 families. To determine the pathogenicity of PPFIA3 variants in vivo, we generated transgenic fruit flies producing either human PPFIA3 wildtype (WT) or five missense variants using GAL4-UAS targeted gene expression systems. In the fly overexpression assays, we found that the PPFIA3 variants in the N-terminal coiled-coil domain exhibited stronger

	phenotypes compared to those in the C-terminal region. In the loss-of-function fly assay, we show that the homozygous loss of fly Liprin-α leads to embryonic lethality. This lethality is partially rescued by the expression of human PPFIA3 WT, suggesting human PPFIA3 function is partially conserved in the fly. However, two of the tested variants failed to rescue the lethality at the larval stage and one variant failed to rescue lethality at the adult stage. Altogether, the human and fruit fly data reveal that the rare PPFIA3 variants are dominant negative loss-of-function alleles that perturb multiple developmental processes and synapse formation.

A syndromic neurodevelopmental disorder caused by rare variants in *PPFIA3*

Maimuna S. Paul[1,2,3], Sydney L. Michener[1,2,3], Hongling Pan[2,4], Hiuling Chan[3,5,6], Jessica M. Pfliger[1,2,7], Jill A. Rosenfeld[4], Vanesa C. Lerma[1,2,8], Alyssa Tran[4], Megan A. Longley[1,2], Richard A. Lewis[4,9], Monika Weisz-Hubshman[4], Mir Reza Bekheirnia[4,10], Nasim Bekheirnia[10], Lauren Massingham[11], Michael Zech[12,13, 14], Matias Wagner[12,13,15], Hartmut Engels[16], Kirsten Cremer[15], Elisabeth Mangold[15], Sophia Peters[15], Jessica Trautmann[15], Jessica L. Mester[17], Maria J. Guillen Sacoto[17], Richard Person[17], Pamela P. McDonnell[18,19], Stacey R. Cohen[18], Laina Lusk[18], Ana S.A. Cohen[20], Jean-Baptiste Le Pichon[21], Tomi Pastinen[20,22], Dihong Zhou[23], Kendra Engleman[23], Caroline Racine[24,25], Laurence Faivre[25,26], Sébastien Moutton[25,26], Anne-Sophie Denommé-Pichon[24,25], Hyun Yong Koh[1,27], Annapurna Poduri[27], Jeffrey Bolton[27], Cordula Knopp[28], Dong Sun Julia Suh[28], Andrea Maier[29], Mehran Beiraghi Toosi[30,31], Ehsan Ghayoor Karimiani[32,33], Reza Maroofian[34], Gerald Bradley Schaefer[35], Vijayalakshmi Ramakumaran[36], Pradeep Vasudevan[36], Chitra Prasad[37], Matthew Osmond[38], Sarah Schuhmann[39], Georgia Vasileiou[39], Sophie Russ-Hall[40], Ingrid E. Scheffer[40,41], Gemma L. Carvill[42], Heather Mefford[43], Undiagnosed Diseases Network, Carlos A. Bacino[4,44], Brendan H. Lee[4,44], Hsiao-Tuan Chao[1,2,3,4,44,45,46]

Author affiliations:

[1]Department of Pediatrics, Section of Neurology and Developmental Neuroscience, Baylor College of Medicine, Houston, TX, USA; [2]Jan and Dan Duncan Neurological Research Institute, Texas Children's Hospital, Houston, TX, USA; [3]Cain Pediatric Neurology Research Foundation Laboratories, Jan and Dan Duncan Neurological Research Institute, Houston, TX, USA; [4]Department of Molecular and Human Genetics, Baylor College of Medicine, Houston, TX, USA; [5]Augustana College, Rock Island, Illinois, USA; [6]Summer Undergraduate Research Training (SMART) Program, Baylor College of Medicine, Houston, TX, USA; [7]Graduate Program in Electrical and Computer Engineering, Rice University, Houston, TX, USA; [8]Department of Psychology, University of Houston, Houston, Texas, USA; [9]Department of Ophthalmology, Baylor College of Medicine, Houston, TX, USA; [10]Renal Genetics Clinic, Baylor College of Medicine, Houston, TX, USA; [11]Rhode Island Hospital and Hasbro Children's Hospital, Providence, RI, USA; [12]Institute of Neurogenomics, Helmholtz Zentrum München, Munich, Germany; [13]Institute of Human Genetics, School of Medicine, Technical University, Munich, Germany; [14]Institute for Advanced Study, Technical University of Munich, Garching, Germany; [15]Division of Pediatric Neurology, Developmental Neurology and Social Pediatrics, Dr. von

35 Hauner Children's Hospital; [16]Institute of Human Genetics, School of Medicine, University
36 Hospital Bonn, University of Bonn, Bonn, Germany; [17]GeneDx Gaithersburg, MD, USA;
37 [18]Epilepsy NeuroGenetics Initiative (ENGIN), Division of Neurology, Children's Hospital of
38 Philadelphia, Philadelphia, PA, USA; [19]Department of Neurology, Perelman School of Medicine,
39 University of Pennsylvania, PA, USA; [20]Children's Mercy Kansas City, Genomic Medicine
40 Center, The University of Missouri-Kansas City (UMKC), School of Medicine, Kansas City, MO,
41 USA; [21]Department of Pediatrics, Children's Mercy Kansas City, Kansas City, MO; [22]Children's
42 Mercy Research Institute, Kansas City, MO; [23]Children's Mercy Hospital, Kansas City, MO,
43 USA; [24]University Hospital, Dijon, France INSERM UMR1231 GAD "Génétique des Anomalies
44 du Développement," FHU-TRANSLAD, University of Burgundy, Dijon, France; [25]Functional Unit
45 for Diagnostic Innovation in Rare Diseases, FHU-TRANSLAD, Dijon Bourgogne; [26]Department
46 of Genetics and Reference Center for Development Disorders and Intellectual Disabilities, FHU-
47 TRANSLAD and GIMI Institute, Dijon Bourgogne University Hospital, Dijon, France;
48 [27]Department of Neurology, Boston Children's Hospital, Boston, MA, USA; [28]Institute for Human
49 Genetics and Genomic Medicine, Medical Faculty, RWTH, Aachen University, Aachen,
50 Germany; [29]Medical Treatment Center for Adults with Intellectual Disabilities and/or Severe
51 Multiple Disabilities (MZEB), RWTH Aachen University Hospital, Aachen, Germany;
52 [30]Department of Pediatrics, School of medicine, Mashhad university of medical sciences,
53 Mashhad, Iran; [31]Neuroscience Research Center, Mashhad University of Medical Sciences,
54 Mashhad, Iran; [32]Department of Medical Genetics, Next Generation Genetic Polyclinic,
55 Mashhad, Iran; [33]Molecular and Clinical Sciences Institute, St. George's, University of London,
56 Cranmer Terrace, London, UK; [34]Department of Neuromuscular Diseases, UCL Queen Square
57 Institute of Neurology, London, United Kingdom; [35]University of Arkansas For Medical Sciences;
58 Little Rock, AR, USA; [36]LNR Genomics Medicine, University Hospitals of Leicester, UK;
59 [37]London Health Sciences Centre, and Division of Medical Genetics, Department of Pediatrics,
60 Western University, London, ON, Canada; [38]Children's Hospital of Eastern Ontario Research
61 Institute, University of Ottawa, ON, Canada; [39]Institute of Human Genetics, Universitätsklinikum
62 Erlangen, Friedrich-Alexander-Universität Erlangen-Nürnberg, Erlangen, Germany; [40]Epilepsy
63 Research Centre, Department of Medicine, University of Melbourne, Austin Health, Victoria,
64 Australia; [41]Department of Pediatrics, University of Melbourne, Royal Children's Hospital, Florey
65 and Murdoch Children's Research Institutes, Melbourne, Australia; [42]Department of Neurology,
66 Northwestern University Feinberg School of Medicine, Chicago, IL, USA; [43]Center for Pediatric
67 Neurological Disease Research, St. Jude Children's Research Hospital, Memphis, TN, USA;
68 [44]Texas Children's Hospital, Houston, TX, USA; [45]Department of Neuroscience, Baylor College

of Medicine, Houston, TX, USA; [46]McNair Medical Institute, The Robert and Janice McNair Foundation, Houston, TX, USA

Correspondence to Hsiao-Tuan Chao
Full address: Jan and Dan Duncan Neurological Research Institute, 1250 Moursund St, Suite 925, Houston, TX, 77030
Tel: 832-822-5046
E-mail: chao-lab@bcm.edu

RUNNING TITLE: *PPFIA3* variants in neurodevelopmental disorder

KEYWORDS: Neurodevelopmental disorder; Synaptic protein; Active zone protein; Mendelian phenotypes; Fruit flies

ABSTRACT

PPFIA3 encodes the Protein-Tyrosine-Phosphatase, Receptor-Type, F-Polypeptide-Interacting-Protein-Alpha-3 (PPFIA3), which is a member of the LAR-protein-tyrosine phosphatase-interacting-protein (liprin) family involved in synapse formation and function, synaptic vesicle transport, and presynaptic active zone assembly. The protein structure and function are evolutionarily well-conserved, but human diseases related to PPFIA3 dysfunction are not yet reported in OMIM. Here, we report 20 individuals with rare *PPFIA3* variants (19 heterozygous and 1 compound heterozygous) presenting with developmental delay, intellectual disability, hypotonia, dysmorphisms, microcephaly or macrocephaly, autistic features, and epilepsy with reduced penetrance. Seventeen unique *PPFIA3* variants were detected in 18 families. To determine the pathogenicity of *PPFIA3* variants *in vivo*, we generated transgenic fruit flies producing either human PPFIA3 wildtype (WT) or five missense variants using GAL4-UAS targeted gene expression systems. In the fly overexpression assays, we found that the *PPFIA3* variants in the N-terminal coiled-coil domain exhibited stronger phenotypes compared to those in the C-terminal region. In the loss-of-function fly assay, we show that the homozygous loss of fly *Liprin-α* leads to embryonic lethality. This lethality is partially rescued by the expression of human *PPFIA3* WT, suggesting human PPFIA3 function is partially conserved in the fly. However, two of the tested variants failed to rescue the lethality at the larval stage and one variant failed to rescue lethality at the adult stage. Altogether, the human and fruit fly data reveal

that the rare *PPFIA3* variants are dominant negative loss-of-function alleles that perturb multiple developmental processes and synapse formation.

INTRODUCTION

Synapses are highly specialized communication junctions between neurons and their target cells where, neurotransmitter release occurs in an intricately coordinated manner. In the presynaptic neuron, a key site for neurotransmitter release is the active zone, which is composed of a complex protein matrix.[1–4] RIM, ELKS, Munc13, RIM-BP, Piccolo/Bassoon, and Liprin-α are the six major protein families comprising the active zone.[5] These active zone proteins along with other cytoskeletal proteins, Ca^{2+} channels, and SNAREs (soluble N-ethylmaleimide-sensitive fusion protein attachment protein receptors) form a tightly orchestrated unit to mediate synaptic vesicle docking, priming, fusion, and neurotransmitter release.[5] Prior studies revealed that disruption of synapse structure or function leading to variable defects in neurotransmitter release contributes to neurodevelopmental and neuropsychiatric disorders including epilepsy, intellectual disability (ID), autism spectrum disorder (ASD), schizophrenia, and bipolar disorder.[6–10]

The network of multidomain proteins comprising the active zone falls into different categories such as cytoskeletal and scaffolding proteins, adhesion molecules, calcium channels, and synaptic vesicle release machinery. Liprins are scaffolding proteins found in the presynaptic active zone that are also known as protein-tyrosine phosphatase, receptor-type, f polypeptide (PTPRF)-interacting protein α (PPFIA) or β (PPFIB). Liprin family members interact with the adhesion molecule LAR-PTPs (Leukocyte Antigen Receptor-Protein Tyrosine Phosphatases) and are subdivided into liprin-α and liprin-β proteins.[11,12] In conjunction with LAR-PTPs, liprins play a key role in the active zone organization and structure. Structural studies show that liprins, including PPFIA3, are comprised of an N-terminal coiled-coil domain and C-terminal sterile-α-motif (SAM) domain.[11,12] The N-terminal coiled-coil domain mediates homodimerization and heterodimerization with other liprin-α members and interactions with other active zone proteins such as RIM and ELKS.[13–16] The SAM domains are known for mediating protein-protein interactions and binding with RNA.[17] The liprin-α SAM domain interacts with the LAR intracellular domain.[18] Apart from these functional domains, liprins also contain intrinsically disordered regions that lack an ordered three-dimensional structure but were previously shown to be important for protein's function.[19,20] Additionally, liprins interact with kinesin motor proteins[21–23] and are involved in the hedgehog signaling-dependent trafficking of Kif7 and Gli to the cilia in the context of embryonic development and cortical microtubule organization.[21,22]

136 Vertebrates have four Ppfia (1-4) and two Ppfib (1-2) that are encoded by *Ppfia1-4* or *Ppfib1-2*
137 respectively.[12] Expression studies in mice show that all four mouse Ppfia1-4 homologs are
138 expressed in the brain, with differences in distribution and expression levels.[24] Ppfia1 is found in
139 the brain, lung, heart, liver, muscle, spleen, and testes.[12,25,26] In the brain, Ppfia1 is
140 predominantly localized to the cerebellum and olfactory bulb.[24–26] In contrast, Ppfia2, Ppfia3,
141 and Ppfia4 are predominantly found in the brain,[12,25,26] including structures such as the olfactory
142 bulb, striatum, cortex, hippocampus, thalamus, midbrain, cerebellum, and brainstem.[24–26] A
143 subcellular localization study showed that Ppfia2 and Ppfia3 are located in both the pre-synaptic
144 and post-synaptic compartments.[26] However, only Ppfia3 specifically colocalizes in the
145 presynaptic compartment and mediates protein-protein interactions with the active zone proteins
146 Bassoon, RIM, Munc-13, RIM-BP, and ELKS in hippocampal neurons.[27] In humans,
147 transcriptomic studies revealed that *PPFIA3* (MIM*603144) is similarly expressed in different
148 brain regions like the neocortex, striatum, hippocampus, amygdala, mediodorsal nucleus of the
149 thalamus, and cerebellar cortex from the early embryonic stage to late adulthood.[28]

150 Ppfia proteins are well conserved in both vertebrates and invertebrates. In *C. elegans*, the sole
151 Ppfia homolog, syd-2, plays a key role in presynaptic active zone organization.[29,30] Studies
152 showed that syd-2 recruits synaptic components to presynaptic sites and contributes to the
153 formation of neuromuscular junctions (NMJs), along with active zone assembly and
154 stabilization.[30,31] Mutant syd-2 worms show presynaptic active zone defects due to disruption of
155 syd-2 oligomerization.[13,30,31] A similar role was found for the fruit fly homolog, Liprin-α, where it is
156 required for synapse formation, synaptic vesicular transport, active zone assembly, and axonal
157 target selection from the retina to the medulla in the central nervous system.[32–34] Consistent with
158 the invertebrate models, synaptic ultrastructure and electrophysiological studies in *Ppfia3*
159 knock-out mice found impaired presynaptic active zone assembly, synaptic vesicle docking,
160 tethering, and exocytosis.[27] Altogether, these studies reveal that Ppfia family members are
161 integral scaffolding proteins for the assembly of intricate protein complexes involved in synapse
162 formation, synaptic transmission, and protein trafficking.

163 Here, we report a cohort of 20 individuals from 18 families with rare variants in *PPFIA3*
164 associated with developmental delay (DD), intellectual disability (ID), dysmorphisms,
165 microcephaly, macrocephaly, hypotonia, autism spectrum disorder (ASD) or autistic features,
166 abnormal electroencephalogram (EEG), and epilepsy. The phenotypic consequences of rare
167 variants in *PPFIA3* have not been previously reported in OMIM (Online Mendelian Inheritance in
168 Man).[35] In a statistical model of *de novo* variants for autism spectrum and intellectual disability

169 disorders (ASD/ID), *PPFIA3* was identified as one of ~1,000 genes significantly lacking
170 functional variation in non-ASD/ID individuals but are enriched with *de novo* variants in ASD/ID
171 individuals.[36] Furthermore, gnomAD v2.1.1 analysis showed that *PPFIA3* has a high probability
172 of loss-of-function (LOF) intolerance (LOEUF = 0.12, pLI = 1.0), as 64.1 LOF variants were
173 expected given the gene size and GC content but only three LOF variants were observed.[37]
174 *PPFIA3* is also a highly constrained gene with a missense z-score of 5.49, suggesting
175 intolerance to missense variation, as 727.5 missense variants were expected but only 311 were
176 observed.[37] Together, these findings support that rare *PPFIA3* variants may cause a
177 neurodevelopmental phenotype.

178 The pathogenicity of the five *PPFIA3* missense variants were tested using overexpression fly
179 assays, revealing that the *PPFIA3* variants are associated with behavioral, developmental, and
180 NMJ defects. Loss-of-function (LOF) assays with fly *Liprin-α* show that the human *PPFIA3*
181 wildtype (WT) partially rescued the *Liprin-α* LOF embryonic lethality whereas three of the five
182 tested variants exhibited impaired rescue of the LOF phenotype. Altogether, we show that rare
183 *PPFIA3* variants are deleterious to protein function with *in vivo* fruit fly assays and lead to a
184 syndromic neurodevelopmental disorder characterized by DD, ID, hypotonia, ASD or autistic
185 features, dysmorphisms, microcephaly or macrocephaly, abnormal EEG, and epilepsy in
186 humans.

187

188 **MATERIAL AND METHODS**

189 **Study approval for Identification of study participants and clinical phenotyping**

190 Clinical data were acquired after written informed consent was obtained in accordance with the
191 ethical standards of the participating institutional review boards (IRB) on human research at
192 each respective institution. GeneMatcher was used to form an international collaboration,
193 allowing for comparison of individuals and their variants.[38–40] Collection and analysis of the de-
194 identified clinical cohort was approved by Baylor College of Medicine's IRB. *PPFIA3*
195 heterozygous variants were identified by ES through each individual's respective institution.
196 DNA was extracted from peripheral blood mononuclear cells, buccal sample, or fetal skin for
197 ES. Exome or Sanger sequencing of the parental samples were performed when feasible to
198 confirm *de novo* or inherited segregation. Paternity was confirmed by the inheritance of rare
199 single nucleotide polymorphisms from the parents. Sample swap was excluded. Participant ID's
200 are not known to anyone outside of the research group. Clinical phenotypes are ascertained by
201 expert review of medical records and the most recent clinical assessment per each individual.

202

203 **Molecular modeling**

204 Molecular visualization of the PPFIA3 structure was completed with PyMol (The PyMOL
205 Molecular Graphics System, Version 2.5.2 Schrödinger, LLC.). The crystal structure of PPFIA3
206 (GenBank NP_003651.1, Uniprot ID: O75145) was used to build the PPFIA3 structure model in
207 PyMol. Affected residues were altered to the corresponding human variants and the mutation
208 effects were modeled alongside the native protein. The changes in the PPFIA3 structure was
209 assessed by displaying local polar contacts and residue interactions before and after
210 mutagenesis.

211

212 ***Drosophila melanogaster* stocks and maintenance**

213 All the fruit fly stocks used in this study were reared in standard cornmeal and molasses-based
214 fly food at room temperature (RT, 20-21°C) unless otherwise noted. The fruit fly stocks used in
215 the study were either obtained from Bloomington Drosophila Stock Center (BDSC) or generated
216 at the Jan and Dan Duncan Neurological Research Institute. We generated transgenic fly alleles
217 as previously described[41] by utilizing the pUASg-HA-attB vector[42] to express the human *PPFIA3*
218 WT and variant cDNAs with a C-terminal hemagglutinin (HA) tag under the control of Upstream
219 Activating Sequence (UAS) elements by Gateway LR Cloning (LR Clonase II, Thermo Fisher
220 Scientific, Cat #11791020). To generate the *PPFIA3* variants, we utilized the human full-length
221 cDNA of *PPFIA3* (GenBank: NM_003660.4). *PPFIA3* c.115 C>T [p.(Arg39Cys)], *PPFIA3*
222 c.943G>T [p.(Ala315Ser)], *PPFIA3* c.1243C>T [p.(Arg415Trp)], *PPFIA3* c.1638G>T
223 [p.(Trp546Cys)], and *PPFIA3* c.2350C>T [p.(Arg784Trp)] were generated by Q5 site-directed
224 mutagenesis (New England Biolabs, Cat #M0491S) in the pDONR221 Gateway compatible
225 donor vector. The constructs were confirmed by Sanger sequencing. Primer sequences for the
226 site-directed mutagenesis and Sanger sequencing are listed in **Table S1**. Human *PPFIA3* WT
227 and variant cDNAs were inserted into the chromosome-3 VK33 (PBac{y[+]-attP}VK00033)
228 docking site by *φ*C31-mediated recombination for fruit fly transgenesis.[42] Transgenic UAS fly
229 alleles generated in this study include *UAS-PPFIA3*-WT-HA*, UAS-PPFIA3*-p.(Arg39Cys)-HA*,*
230 *UAS-PPFIA3*-p.(Ala315Ser)-HA*, UAS-PPFIA3*-p.(Arg415Trp)-HA*, UAS-PPFIA3*-p.(Trp546Cys)-
231 HA*,* and *UAS-PPFIA3*-p.(Arg784Trp)-HA. Fly alleles from the stock centers include: *Liprin-*
232 *α^{F3ex15}/In(2LR)Gla* (BDSC#8563), *w[1118]; Df(2L)Exel7027/CyO* (BDSC#7801), *y[1] w[118];*
233 *PBac{y[+]-aatP-3B}-VK00033* (BDSC#9750), and *elav-GAL4/CyO* (BDSC#8765). *UAS*-empty-
234 *VK33, Actin-GAL4,* and *da-GAL4* lines were obtained from Dr. Hugo J. Bellen.

235

236

237 **Larval brain and NMJ immunostaining and confocal microscopy**

238 Fruit fly larval brains or whole-body wall muscles including the central nervous system were
239 dissected from wandering third instar larvae reared at 25ºC in ice-cold 1X-PBS and fixed in 4%-
240 paraformaldehyde for 20 minutes at RT. The tissues were washed four times in Tri-PBS (1X-
241 PBS + 0.2% Triton-X-100) with 1%-Bovine Serum Albumin (BSA) for 15-minutes each followed
242 by incubation in blocking solution (Tri-PBS with 0.1% BSA and 8% normal donkey serum) for 30
243 minutes. Primary antibodies, rat anti-HA (1:50, clone 3F10, Millipore Sigma, Cat#11867423001),
244 mouse anti-elav (1:100, Developmental Studies Hybridoma Bank, Cat#9F8A9), mouse anti-
245 Bruchpilot (Brp) (1:50, Developmental Studies Hybridoma Bank, Cat#nc82), and goat anti-
246 Horseradish Peroxidase (HRP) (1:1000, Jackson ImmunoResearch, Cat#123-005-021) were
247 diluted in blocking solution, added to the tissues, and incubated overnight at 4°C. The tissues
248 were rinsed three to four times in Tri-PBS with 1%-BSA for 15-minutes each followed by
249 incubation in blocking solution for 30 minutes at RT. The secondary antibodies, donkey anti-rat
250 IgG antibody (Cy3) (1:300, Jackson ImmunoResearch, Cat#712-165-153), Alexa Fluor 488
251 Affinipure donkey anti-goat IgG (H+L) (1:300, Jackson ImmunoResearch, Cat#705-545-147)
252 and Alexa Fluor 488 Affinipure donkey anti-mouse IgG (H+L) (1:300, Jackson
253 ImmunoResearch, Cat#715-545-151) were diluted in blocking solution and added to the tissues
254 for a 90-minute incubation at RT on a rocker. For NMJ staining, phalloidin (Phalloidin-iFluor 405
255 Reagent, Abcam, Cat#ab176752) was added along with the secondary antibodies to visualize
256 the muscles. After removing the secondary antibody, tissues were washed three times in Tri-
257 PBS with 1% BSA for 15-minutes each, and then rinsed in 1X-PBS at RT. For larval brains, this
258 was followed by incubation in 406-diamidino-2-phenylindole dihydrochloride (DAPI, 1 mg/mL,
259 Cayman Chemical, Cat#14285) for 30-minutes at RT. After removing DAPI, a final wash was
260 completed with 1X-PBS for 15-minutes at RT. The tissues were mounted in Prolong Glass anti-
261 fade mountant (Thermo Scientific, Cat#36984). Images were acquired on a Leica Sp8 laser-
262 scanning confocal microscope. The same settings for laser power and detector gain were used
263 for all genotypes. Third instar larval brain images were acquired as a z-stack with a z-step of
264 1μm and line average of four at 400 Hz with a 20X objective at 1024 x 1024-pixel resolution.
265 NMJ images were acquired with a 40X objective. Maximum intensity projections were created
266 from the z-stack in ImageJ. All images were processed and assembled using ImageJ and
267 Adobe Illustrator.

268

269

270 **Western blotting**

271 Adult fly heads were homogenized using cell lysis buffer (50mM Tris-HCl, 150mM NaCl, 0.25%
272 SDS, 0.25% sodium deoxycholate, 1mM EDTA, and 1X liquid protease inhibitor (Gen DEPOT
273 Cat#P3100-001). The homogenized fly heads in cell lysis buffer were centrifuged at 13,000 rpm
274 for 10-minutes at 4°C. The supernatant was collected and mixed with Laemmli buffer containing
275 β-mercaptoethanol and heated at 95°C for 10-minutes. The samples were loaded in 4–20%
276 gradient polyacrylamide gels (Bio-Rad MiniPROTEAN® TGXTM Cat# 4561086) followed by a
277 transfer onto polyvinylidene difluoride membrane (Bio-Rad TransBlot Turbo mini-size LF PVDF
278 membrane). The membrane was blocked using skim milk and treated overnight with the primary
279 antibody (rat anti-HA 1:2000, clone 3F10, Millipore Sigma, Cat#11867423001). Anti-actin hFAB™
280 rhodamine antibody (Bio-Rad Cat#12004163, 1:5000) and goat anti-rat IgG polyclonal antibody
281 (IRDye® 800CW) (LI-COR Biosciences, Cat#926-32219) were used as the secondary antibodies.
282 Images were acquired on the BioRad Chemidoc Imaging System (Cat#17001401). Quantification
283 was done using ImageJ in which background subtracted band intensity is acquired for both the
284 actin and HA bands. The average intensity value is normalized and analyzed in GraphPad Prism8.
285 Crosses for the Western blot analysis were set up and maintained at 25°C.
286

287 **Third instar larval NMJ quantifications**

288 The total number of boutons from abdominal segment A3, muscle 6/7 were counted semi-
289 manually using Imaris. The spot function was used with point style sphere and radius scale 1.0
290 to count the number of boutons. The NMJ length was quantified using the HRP staining and
291 measured in ImageJ.
292

293 **Fruit fly behavioral assays**

294 For the climbing assay, 5-day-old flies of both sexes were anesthetized with CO_2 48-hours prior
295 to being tested and two to three flies were housed in food-containing vials at 25°C. At the time
296 of assay, these flies were transferred without anesthesia to a clear graduated cylinder with a 15-
297 cm mark. The flies were tapped three times to the bottom of the cylinder to examine the
298 climbing ability. The cutoff time to reach the 15-cm mark was 30-seconds. A total of 55-75 flies
299 of both sexes were tested for each genotype. Crosses for the climbing assay were set up at
300 25°C and the assay was performed at 20-21°C. The climbing assay for 15-day old flies was
301 done with the flies anesthetized with CO_2 24-hours prior to being tested and kept at room
302 temperature until the behavioral test was done. The cutoff time for the 15-day old flies to reach

303 the 20-cm mark was 40-seconds. A total of 40-55 flies of both sexes were tested for each
304 genotype for the 15-day old flies.
305
306 For the bang sensitivity assay, 5-day-old flies of both sexes were anesthetized with CO_2 48-
307 hours prior to being tested and two to three flies were housed in food-containing vials at 25°C.
308 At the time of assay, these flies were transferred without anesthesia to an empty food vial and
309 vortexed for 10-seconds. Flies were observed for time to recover from the vortexing. The cutoff
310 time to recover was 30-seconds. Recovery was defined as being upright and mobile. Flies were
311 considered bang sensitive if they remained upside down, immobile, or showing rhythmic
312 involuntary movements suggestive of electrophysiological abnormalities in the nervous system.
313 A total of 55-75 flies of both sexes were tested for each genotype. Crosses for the bang
314 sensitivity assay were set up at 25°C and the assay was performed at 20-21°C. The bang
315 sensitivity assay for 15-day old flies was done with the flies anesthetized with CO_2 24-hours
316 prior to being tested and kept at room temperature until the behavioral test was done. The
317 vortexing time for the 15-day old flies was 15-seconds. A total of 40-55 flies of both sexes were
318 tested for each genotype for the 15-day old flies.
319
320 ***Liprin-α* loss-of-function lethality rescue with human PPFIA3 WT and variants**
321 *Df(Liprin-α)/CyO act-GFP; UAS-cDNA/TM6B* flies were crossed with *Liprin-α* ^{F3ex15}*/CyO act-*
322 *GFP; da-GAL4/TM6B* flies. The UAS-cDNA lines used were *UAS*-empty, *UAS-PPFIA3* WT,
323 *UAS-PPFIA3* p.Arg39Cys, *UAS-PPFIA3* p.Arg415Trp, *UAS-PPFIA3* p.Trp546Cys, and *UAS-*
324 *PPFIA3* p.Arg784Trp. Rescue larvae with the genotype, *Df(Liprin-α)/Liprin-α* ^{F3ex15}; *UAS-*
325 *cDNA/da-GAL4* were selected (GFP -ve and non Tb) and kept in a new vial to assess the
326 development. The experiment was done in three biological replicates. The crosses were set and
327 maintained at 20°C as the higher temperature (25°C and above) were embryonic lethal with all
328 cDNAs.
329
330 **Pupal lethality and eclosion defect assessment**
331 *Actin-GAL4/Cyo,Tb* females were crossed with the homozygous *UAS-PPFIA3* WT and *UAS-*
332 *PPFIA3* p.(Arg39Cys), p.(Ala315Ser), p.(Arg415Trp), p.(Trp546Cys), and p.(Arg784Trp) males
333 at 25°C. The overexpression progenies were identified based on the absence of the markers,
334 CyO (visible in adults) and Tb (visible in larvae, pupae, and adults). Sample sizes are shown in
335 **Table S2**.
336

337 **Adult fruit fly leg mounting**

338 Adult flies were fixed overnight in ethanol at room temperature and the legs were dissected and
339 mounted using CMCP-10 Macroinvertebrate High Viscosity Mountant (D/S259) (Electron
340 Microscopy Sciences, Cat#18004-02). Leg images were taken using the Leica MZ16
341 stereomicroscope. Images were processed and assembled using Adobe Photoshop CS5.1 and
342 Adobe illustrator. Crosses were set up at 25°C. Sample sizes are shown in **Table S2**.
343

344 **Genomic DNA isolation and qPCR**

345 Genomic DNA was extracted by homogenizing four whole flies in 50mM sodium hydroxide and
346 heating the samples at 95°C for 30 minutes followed by the addition of 1M Tris-HCl (pH 7.5) to
347 stop the lysis. Equal amount (50ng) of DNA for each genotype was used for amplification. q-
348 PCR was performed with the BioRad SsoAdvanced Universal SYBR-Green Supermix
349 (Cat#1725274) and the BioRad CFX96 Touch Real-Time PCR detection system
350 (Cat#1845096). The relative change in gene expression was determined by the Livak method
351 and fold changes were calculated using the $2^{-\Delta\Delta CT}$ formula. The experiment was repeated in
352 three independent biological replicates. *HA* and *PPFIA3* band intensity were quantified by
353 normalizing to the band intensity of the endogenous reference *rps17* and plotted as fold-change
354 relative to the control. Flies were maintained at 20-21°C. Primer sequences are listed in **Table**
355 **S1**.
356

357 **Statistics**

358 Data was collected and analyzed blinded to genotypes. Statistical analysis between the control
359 and experimental groups was conducted with one-way ANOVA and Tukey's post-hoc analysis
360 in GraphPad Prism 8. Statistical summary is in **Table S3**.

361

362 **RESULTS**

363 **Identification of rare *PPFIA3* variants in individuals with neurodevelopmental phenotypes**

364 An international collaboration through the Undiagnosed Diseases Network (UDN)[43] and
365 GeneMatcher[38–40] led to the identification of 20 individuals from 18 families with
366 neurodevelopmental phenotypes and 17 rare missense, frameshift deletion, exonic deletion, or
367 consensus splice site variants in *PPFIA3* (**Table 1**, **Figure 1A, B, see Supplemental Note**).
368 The cases were ascertained in individuals with phenotypes including DD, ID, ASD or autistic
369 features, epilepsy, abnormal EEG, hypotonia, dysmorphisms, microcephaly, and macrocephaly.

370 Heterozygous *PPFIA3* variants were identified in nineteen individuals (1-19). One individual (20)
371 was found to carry compound heterozygous variants with concordant phenotypes. The variants
372 from all affected individuals were identified through exome sequencing (ES) or Sanger
373 sequencing.
374
375 Eleven of the individuals harbored *de novo* (1-2, 7-8, 10-15, and 17) missense variants. The *de*
376 *novo* p.(Arg429Trp) variant was seen in individual 10 in a mosaic state (present in 26% of the
377 ES reads, suggesting heterozygosity in ~52% of cells) from DNA analysis of fetal skin.
378 Individuals 14 and 15 are monozygotic twins from family 13 and one individual (5) inherited a
379 consensus splice variant from a similarly affected parent (6) (both from family 5). Individual 19
380 inherited a deletion of exons 22-30 from an affected parent, individual 20 inherited compound
381 heterozygous variants from unaffected parents, and the inheritance pattern for six affected
382 individuals is unknown (3, 4, 6, 9, 16, and 18) (**Table 1, see Supplemental Note**). The
383 individuals with unknown inheritance pattern have either a missense variant (3, 4, and 9), a
384 consensus splice variant (6), or a frameshift deletion (16 and 18).
385
386 To determine the potential pathogenicity of the *PPFIA3* variants, we examined the Combined
387 Annotation Depletion (CADD) Score where scores above 20 are considered to be deleterious.[44]
388 The CADD scores for the *PPFIA3* variants ranged from 22.6 to 54, suggesting they are
389 potentially deleterious (**Table 2**). Fourteen out of seventeen variants were absent from the
390 Genome Aggregation Database (gnomAD v2.1.1).[37] The p.(Arg784Trp) variant had a frequency
391 of 3.19×10^{-5} (1/31,386) in gnomAD v2.1.1 and was identified as a *de novo* finding in individual
392 13 with mild ID and Landau-Kleffner epilepsy syndrome. The p.(Pro793Thr) variant had a
393 frequency of 7.61×10^{-4} (215/282,366) in gnomAD v2.1.1 and was identified as a maternally
394 inherited variant in trans with a paternally inherited p.(Lys759Arg) variant in individual 20 with
395 DD, ID, hypotonia, epilepsy, microcephaly, and autistic features. The p.(Lys759Arg) variant has
396 a frequency of 4.77×10^{-5} (13/282,880) in gnomAD v2.1.1. Differences in variant frequencies
397 were documented in gnomAD v.4.0.0, encompassing variants reported in this study that were
398 either submitted to ClinVar or identified from the UK Biobank **(Table S4, S5)**.
399
400 Eighteen individuals in the cohort had DD and ID (1-6, 8-9, 11-20) (**Tables S4, S5, see**
401 **Supplemental Note**), while two individuals (7 and 10) could not be assessed for this feature
402 due to premature mortality. Individual 7 had renal failure, severe anorectal malformation with
403 complete anal atresia, absent bladder, dysmorphisms, and passed away at 5 months of age.

404 Individual 10 had a prenatal diagnosis of abnormal gyration and ventriculomegaly, which led to
405 elective pregnancy termination. Abnormal EEG (seen in 9/20; 1-3, 8, 9, 13, 17, 18, 20) and
406 epilepsy (seen in 6/20; 1-3, 8, 13, 20) were found in a total of nine individuals (**Table 1, see**
407 **Supplemental Note**). The affected individuals had multiple seizure semiologies including focal
408 clonic seizures, atonic seizures, absence seizures, and focal tonic-clonic seizures with
409 secondary generalization (**Tables S4, S5, see Supplemental Note**). Six individuals had
410 neuroanatomical changes detected by MRI (2, 3, 8, 10, 15, 20), which included flattening of the
411 posterior globes at the level of optic nerve insertion, abnormal gyration with ventriculomegaly,
412 and mild periventricular leukomalacia with mild white matter volume loss (**Tables S4, S5)**.
413 Delayed speech development was present in sixteen individuals (1-5, 8, 9, 11, 13-20) with
414 absent speech in two individuals (8 and 20) (**Tables S4, S5, S6, see Supplemental Note**).
415 Hypotonia was present in eight individuals (1, 4, 8, 15, 17-20) (**Tables S4, S5, see**
416 **Supplemental Note**). Co-morbid ASD diagnosis was reported in four individuals (11, 12, 14,
417 17) (**Table 1, see Supplemental Note**). Five of the individuals had autistic features but no
418 formal diagnosis of autism was made (4, 8, 9, 16, 20) (**Table 1, see Supplemental Note**).
419 Gastrointestinal dysmotility characterized by constipation, difficulty feeding, and dysphagia was
420 present in ten individuals (1, 3, 4, 7-9, 13-15, 20) (**Tables S4, S5, see Supplemental Note**).
421 Dysmorphic facial features were described in thirteen individuals, which included prominent
422 forehead, plagiocephaly, triangular face, clinodactyly, strabismus, wide mouth, widely spaced
423 teeth, and bilateral epicanthal folds (1-5, 7-9, 11, 17-20) (**Table 1, Table S4, S5, Figure 1C, see**
424 **Supplemental Note**). Macrocephaly or microcephaly were present in nine individuals (5-8, 14,
425 15, 17, 19, 20) (**Table S4, S5, see Supplemental Note**).
426
427 **Conservation analysis and molecular modeling of *PPFIA3* variants**
428 The predicted pathogenicity of *PPFIA3* variants was validated *in vivo* using *D. melanogaster*
429 (fruit fly). The fly homolog of *PPFIA3* is *Liprin-α*, and the fly protein shows an overall 48%
430 identity and 62% similarity with the human protein (**Figure 1B**). Like the human PPFIA3, the fruit
431 fly Liprin-α contains N-terminal coiled-coil domains and three C-terminal SAM domains (**Figure**
432 **1B**). Seven of the variants, p.(Arg39Cys), p.(Glu40Lys), p.(Gln80Pro), p.(Ala315Ser),
433 p.(Arg415Trp), p.(Arg429Trp), and p.(Arg498Trp) are located in the N-terminal coiled-coil
434 domain (**Figure 1B**). The variants p.(Ile870Asn) and p.(Ser903Leufs*86) are located in the
435 SAM1 domain (**Figure 1B**). The variants p.(Trp546Cys), p.(Lys759Arg), p.(Arg784Trp),
436 p.(Pro793Thr), and p.(Ser906Leu) are in the intrinsically disordered region of the protein,
437 however p.(Ser906Leu) is located near the SAM1 domain (**Figure 1B**). Conservation analysis of

438 p.Arg39, p.Gln80, p.Ala315, p.Arg415, and p.Arg429 reveals these coiled-coil domain residues
439 are well-conserved in invertebrates and vertebrates. However, p.Glu40 is only conserved in
440 mice and p.Arg498 is only conserved in mice and worms (**Figure S1**). The affected residues in
441 the SAM1 domain, p.Ile870 and p.Ser903, and the residue near the SAM1 domain, p.Ser906,
442 are also conserved across species. In the intrinsically disordered region, p.Trp546 is conserved
443 in mice, but not in fruit flies and worms; p.Lys759 is conserved in mice and fruit flies; p.Arg784 is
444 conserved only in mice; and p.Pro793 is conserved only in mice (**Figure S1**). The affected
445 variant in the SAM3 domain, p.Glu1103 is conserved in mice and fruit flies, but not in worms
446 (**Figure S1**).
447
448 Molecular modeling was completed for the missense variants using PyMol to determine if the
449 amino acid changes affect protein function *in silico* (**Figure 2A, B**). Regarding the coiled-coil
450 variants, the variant p.(Arg415Trp) introduces a bulky side chain predicted to disrupt the
451 interaction with p.Gln411 (**Figure 2Ai**). Similarly, the variant p.(Arg429Trp) introduces a bulky
452 side chain that may disrupt the interaction with p.Asp424 (**Figure 2Aii**). The variant
453 p.(Arg784Trp) introduces a bulky side chain predicted to disrupt the polar interaction with
454 p.Asp785 (**Figure 2Bi**). The variant p.(Ser906Leu) is near the SAM1 domain and disrupts the
455 interaction with the neighboring residue p.Ser908 (**Figure 2Bii**). Together, the molecular
456 modeling suggests that these rare variants may hinder PPFIA3 function by disrupting the polar
457 interactions with neighboring residues.
458
459 ***In vivo* functional analysis of *PPFIA3* missense variants in fruit flies**
460 To study the functional consequences of *PPFIA3* variants *in vivo*, we selected five of the
461 missense variants to generate transgenic fruit flies using human cDNAs. We generated *UAS-*
462 *PPFIA3*-WT-*HA, UAS-PPFIA3*-p.(Arg39Cys)-*HA, UAS-PPFIA3*-p.(Ala315Ser)-*HA, UAS-*
463 *PPFIA3*-p.(Arg415Trp)-*HA, UAS-PPFIA3*-p.(Trp546Cys)-*HA,* and *UAS-PPFIA3*-p.(Arg784Trp)-
464 *HA* fly alleles with C-terminal HA epitope tags (Table S7). The GAL4-UAS expression system
465 was used to express *PPFIA3* WT and variant cDNAs under the spatiotemporal regulation of the
466 transactivator protein GAL4 (**Figure S2A**). A pan-neuronal driver on the second chromosome,
467 *elav-GAL4*, was used to express *PPFIA3* cDNAs in neurons and a ubiquitous driver on the
468 second chromosome, *Actin-GAL4*, was used to express *PPFIA3* cDNAs in the whole fly (**Figure**
469 **S2A**). We found that *elav-GAL4* and *Actin-GAL4* produced the HA-tagged PPFIA3 WT and
470 variants in 3rd instar larval brains (**Figure S2B**) and adult fly heads (**Figure 2C**). Interestingly,
471 we observed elevated PPFIA3 p.(Arg39Cys) level compared to PPFIA3 WT and the other

472 missense variants (**Figure 2Ci-ii, Figure S3**). To confirm the cDNA copy number insertions are
473 consistent between the *PPFIA3* WT and variant fly lines, genomic DNA qPCR using SYBR
474 Green was performed in *UAS-PPFIA3*-WT-*HA, UAS-PPFIA3*-p.(Arg39Cys)-*HA, UAS-PPFIA3*-
475 p.(Ala315Ser)-*HA, UAS-PPFIA3*-p.(Arg415Trp)-*HA, UAS-PPFIA3*-p.(Trp546Cys)-*HA,* and *UAS-*
476 *PPFIA3*-p.(Arg784Trp)-*HA*. Genomic DNA regions for *HA* epitope tag, *PPFIA3*, and *rps17* were
477 amplified, and the expression levels of either *HA* or *PPFIA3* was quantified using *rps17* as the
478 internal control (**Figures S2Ci-ii**). We also performed semi-quantitative genomic DNA PCR
479 using Taq polymerase and the PCR product band intensity was quantified using *rps17* as the
480 internal control (**Figure S4, S5**). No significant difference in the relative expression of *HA* and
481 *PPFIA3* was observed by both genomic DNA qPCR and PCR analyses, indicating the cDNA
482 copy number is similar across all the *UAS-PPFIA3* WT and variant fly lines. Hence, the higher
483 protein levels observed for p.(Arg39Cys) may be due to increased protein stability from the
484 missense variant.
485
486 To determine if expression of *PPFIA3* WT and missense variants are deleterious to
487 developmental processes, we ubiquitously expressed *PPFIA3* cDNAs using *Actin-GAL4* at 25°C
488 and analyzed the fly development from pupal stage. *PPFIA3* cDNAs were expressed in the
489 presence of endogenous fly *Liprin-α*. We found that *PPFIA3* p.(Arg39Cys) cause pupal lethality
490 and eclosion defects, whereas p.(Ala315Ser) and p.(Arg415Trp) cause only eclosion defect
491 (**Figure 3Ai-ii**). However, these phenotypes were not observed for the *PPFIA3* p.(Trp546Cys)
492 and p.(Arg784Trp) variants that are located in the intrinsically disordered region (**Figure 3Ai-ii**).
493 In the eclosed adult flies, we observed a reduced penetrance of leg dysmorphology. The typical
494 wildtype morphology is comprised of three pairs of legs with each leg containing three
495 segments: femur, tibia, and tarsus (**Figure 3Bi**). We found morphological defects in these
496 segments in either the first, second, third, or all leg pairs with expression of the *PPFIA3*
497 missense variants (**Figure 3Bi**). Leg dysmorphology was observed in 80% of *PPFIA3*
498 p.(Arg39Cys) flies, 50% of *PPFIA3* p.(Ala315Ser) flies, and 40% of *PPFIA3* p.(Arg415Trp) flies
499 (**Figure 3Bi-ii**). In *PPFIA3* p.(Arg784Trp) flies, 10% had leg defects but the phenotype was not
500 significant compared to that of *PPFIA3* WT flies (**Figure 3Bi-ii**). In contrast, the leg
501 dysmorphology phenotype was absent in the *PPFIA3* p.(Trp546Cys) flies (**Figure 3Bi-ii**).
502
503 Next, to determine if the neuronal expression of *PPFIA3* variants by *elav-GAL4* at 25°C
504 impaired nervous system development and function, we conducted climbing behavior, bang
505 sensitivity behavior, and NMJ morphology assays. First, we performed a climbing assay in 5-

506 day old flies to assess for motor defects. The standard behavior of the flies is to climb upward,
507 and any increase in time to climb represents a potential defect in either motor coordination or
508 negative geotaxis. Therefore, we used the climbing assay primarily as a screening tool to
509 assess motor function. We found that *elav-GAL4>UAS-PPFIA3* WT flies had motor function like
510 control flies that do not produce human PPFIA3 (*elav-GAL4>UAS*-empty) (**Figure 4A**).
511 However, climbing behavior was impaired in *PPFIA3* p.(Arg39Cys), p.(Ala315Ser),
512 p.(Arg415Trp), and p.(Arg784Trp) expressing 5-day old flies (**Figure 4A**). Second, to determine
513 if the *PPFIA3* variants have electrophysiological abnormalities in the nervous system, we used
514 bang sensitivity as a screening tool in the 5-day old flies with 10s vortexing. We found that *elav-*
515 *GAL4>UAS-PPFIA3* WT flies were not bang sensitive and recovered similarly to the *elav-*
516 *GAL4>UAS*-empty control. However, p.(Arg39Cys), p.(Ala315Ser), and p.(Arg415Trp) flies
517 exhibited bang sensitivity with an increased recovery time (**Figure 4B**). When we examined the
518 recovery time by sex, we found that p.(Arg39Cys) shows increased recovery time in males
519 (**Figure S6A**), p.(Ala315Ser) shows increased recovery time both in males and females (**Figure**
520 **S6A**), and p.(Arg415Trp) shows increased recovery time in females (**Figure S6A**). To determine
521 if there is an age-dependent effect, the climbing and bang assays were also performed in 15-
522 day old flies. We found that both p.(Arg39Cys) and p.(Arg415Trp) flies had climbing defects
523 (**Figure S6B**). The bang sensitivity assay for 15-day old flies with 15s vortexing showed
524 recovery times similar to the bang sensitivity assay in the 5-day old flies (**Figure S6B**). Third, to
525 explore the consequence of *PPFIA3* variants at the synapse, we examined the fruit fly third
526 instar larval NMJ morphology in muscle 6/7 of abdominal segment 3 (A3) (**Figure 4Ci-ii**). The fly
527 NMJ is a glutamatergic synapse and a well-established model for excitatory glutamatergic
528 synapse development and function[45,46]. We found a reduced number of boutons (presynaptic
529 contacts) with *elav-GAL4* mediated production of the *PPFIA3* p.(Arg39Cys) and p.(Arg415Trp)
530 variants (**Figure 4Ciii**), indicating these variants perturb synapse formation. Total NMJ length
531 associated with the *PPFIA3* variants were like the *PPFIA3* WT and *UAS*-empty controls (**Figure**
532 **4Civ**).
533
534 To determine the functional nature of the human *PPFIA3* variants in the absence of wild-type fly
535 *Liprin-α*, we performed *in vivo* rescue experiments at 20-21°C with a previously established
536 *Liprin-α* LOF allele[32], *Liprin-α*^{F3ex15}, and a *Liprin-α* deficiency allele, *Df(2L)Exel7027/CyO* (**Figure**
537 **5Ai**). To express *PPFIA3* cDNAs in the background of *Liprin-α* LOF, we used the ubiquitously
538 expressing *daughterless-GAL4* (*da-GAL4*). First, we observed that complete loss of *Liprin*-α
539 function (*Liprin-α*^{F3ex15}/*Df(2L)Exel7027*) is embryonic lethal in control *da-GAL4>UAS*-empty flies,

540 with a few escapers reaching larval stage (**Figure 5Aii**). We expressed the human *PPFIA3* WT
541 or variant cDNAs in the background of *Liprin*-α LOF using a ubiquitously expressed *da-GAL4* at
542 20°C and assessed if human *PPFIA3* WT or variants rescued the embryonic lethality. We found
543 a ~25% larval rescue of embryonic lethality with *PPFIA3* WT, indicating functional conservation
544 in fruit flies (**Figure 5Aii**). *PPFIA3* p.(Arg39Cys) and p.(Arg415Trp) resulted in significantly
545 reduced larval rescue compared to WT (8% and 13%, respectively) (**Figure 5Aii**). However, the
546 *PPFIA3* p.(Trp546Cys) and p.(Arg784Trp) variants resulted in ~17% rescue efficiency of the
547 embryonic lethality, which was similar to the *PPFIA3* WT rescue efficiency. Second, we
548 assessed the survival of the rescued larvae to the adult stage (**Figure 5Bi**). We found that
549 ~35% of *PPFIA3* WT larvae reached the adult stage, however none of the *PPFIA3* p.(Arg39Cys)
550 larvae reached the adult stage (**Figure 5Bii**). In contrast, we found that 23% of *PPFIA3*
551 p.(Arg415Trp) larvae reached the adult stage, which is significantly reduced compared to
552 *PPFIA3* WT (**Figure 5Bii**). However, the frequency of *PPFIA3* p.(Trp546Cys) and *PPFIA3*
553 p.(Arg784Trp) larvae reaching the adult stage was similar to *PPFIA3* WT (33% and 30%,
554 respectively) (**Figure 5Bii**). Third, we assessed the survival of these rescue adult flies in the 48
555 hours post-eclosion. We found that 75% of *PPFIA3* WT rescue flies were alive 48 hours post-
556 eclosion, indicating *PPFIA3* WT in the *Liprin-α* LOF background is capable of restoring viability
557 and survival. In contrast, only 35% of the *PPFIA3* p.(Arg415Trp) and 30% of the *PPFIA3*
558 p.(Arg784Trp) rescue flies were alive 48 hours post-eclosion (**Figure 5Biii**). However, *PPFIA3*
559 p.(Trp546Cys) rescue flies had a survival rate similar to *PPFIA3* WT rescue flies **(Figure 5Biii).**
560
561 Finally, we analyzed the number of NMJ boutons and NMJ length with *da-GAL4* mediated
562 production of PPFIA3 WT and variants in the *Liprin-α* LOF background at 20ºC (**Figure S7A**).
563 Although the total number of boutons are significantly reduced compared to *da-GAL4>UAS*
564 empty controls, there is no significant difference in the number of boutons between *PPFIA3* WT
565 and variants (**Figure S7Bi**). We quantified the total length of the NMJ and found no significant
566 difference between genotypes (**Figure S7Bii**). Interestingly, we observed a significantly reduced
567 ratio of bouton numbers per muscle 6/7 NMJ (segment A3) length in both *PPFIA3* WT and
568 variants compared to the *da-GAL4>UAS* empty control (**Figure S7Bii**). However, the bouton to
569 NMJ length ratio remained unchanged between *PPFIA3* WT and variants (**Figure S7Bii**). This
570 indicates that there is a significant loss of bouton density in the background of complete *Liprin-α*
571 LOF compared to the *da-GAL4>UAS* empty control. However, neither *PPFIA3* WT nor variants
572 were able to rescue the loss of NMJ boutons in the *Liprin-α* LOF background (**Figure S7Bi, iii**).
573 It is possible that due to the severity of the complete *Liprin-α* LOF, the *PPFIA3* WT or variants

574 expressing larvae examined for NMJ morphology represent a healthier subset of larvae capable
575 of developing to the 3rd instar stage. Therefore, we may not be capturing *PPFIA3* WT or variants
576 expressing larvae with more severe NMJ phenotypes. This would limit our ability to identify a
577 morphological difference between *PPFIA3* WT and variants in the background of complete
578 *Liprin-α* LOF. Together, the *in vivo* fly functional experiments demonstrate that rare *PPFIA3*
579 variants p.(Arg39Cys), p.(Arg415Trp), and p.(Arg784Trp) result in loss of PPFIA3 function and
580 are deleterious to multiple developmental processes. The clinical findings and fruit fly functional
581 assays show that the *PPFIA3* variants have a variable spectrum of severity. The variants in the
582 coiled-coil domains are associated with multiple neurodevelopment phenotypes in the affected
583 individuals and these variants cause severe phenotypes in the fruit flies as well (**Table 3**).
584 These findings show that rare autosomal dominant or autosomal recessive *PPFIA3* variants in
585 key functional domains may lead to a syndromic neurodevelopmental disorder.
586
587 **DISCUSSION**
588 We describe 20 individuals from 18 families with 17 rare variants in *PPFIA3*, who have
589 neurodevelopmental phenotypes including DD, ID, hypotonia, ASD or autistic features,
590 dysmorphisms, microcephaly or macrocephaly, abnormal EEG, and epilepsy (**see**
591 **Supplemental Note**). The results of our clinical analysis, *in silico* molecular modeling, and *in*
592 *vivo* functional studies in fruit flies show that rare *PPFIA3* variants lead to a syndromic
593 neurodevelopmental disorder. PPFIA3 domain analysis and molecular modeling revealed that
594 seven of the *PPFIA3* missense variants, p.(Arg39Cys), p.(Glu40Lys), p.(Gln80Pro),
595 p.(Ala315Ser), p.(Arg415Trp), p.(Arg429Trp), and p.(Arg498Trp) are located in the N-terminal
596 coiled-coil domain. The coiled-coil domain is critical for PPFIA3's homodimerization and
597 interaction with active zone proteins, such as RIM and ELKS, to regulate active zone
598 organization and synaptic vesicle release.[13–16] Five *PPFIA3* missense variants, p.(Trp546Cys),
599 p.(Lys759Arg), p.(Arg784Trp), p.(Pro793Thr), and p.(Ser906Leu), are located in the intrinsically
600 disordered region of the protein. The p.(Pro793Thr) and p.(Lys759Arg) variants were inherited
601 *in trans* from unaffected parents. One *PPFIA3* missense variant, p.(Ile870Asn), is located in the
602 SAM1 domain. The SAM domains are known to bind to RNA, lipid membranes, and the
603 adhesion molecule LAR-RPTP[18,47,48]. Finally, the *PPFIA3* frameshift deletion variants,
604 p.(Ser903Leufs*86) and p.(Glu1103Asnfs*8), and the exonic deletion variant (Δexons 22-30)
605 may result in nonsense mediated decay followed by reduced protein levels.
606

607 Phenotypic assessment of available clinical information revealed seven commonly reported
608 neurodevelopmental features in the 20 individuals. These seven features include DD, ID,
609 hypotonia, dysmorphisms, microcephaly or macrocephaly, ASD or autistic features, abnormal
610 EEG, and epilepsy (**Tables 1, S4, and S5, see Supplemental Note**). We found that out of the
611 nine individuals with missense variants in the coiled-coil domain (1 and 2, p.(Arg39Cys); 3,
612 p.(Glu40Lys); 4, p.(Gln80Pro); 7, p.(Ala315Ser); 8 and 9, p.(Arg415Trp); 10, p.(Arg429Trp), and
613 11 p.(Arg498Trp)), two individuals had premature mortality (7 and 11). Individuals 1 and 2 have
614 the same variant, p.(Arg39Cys) and share similar clinical features such as abnormal EEG,
615 epilepsy, DD, and ID. Individual 3 had DD, severe ID, hypertonia, dysmorphisms, and epilepsy.
616 Individual 4 had autistic features, DD, ID, hypotonia, and dysmorphisms. Individuals 8 and 9
617 have the same variant, p.(Arg415Trp) in which individual 8 had abnormal EEG, epilepsy, autistic
618 features, DD, ID, hypotonia, dysmorphisms, and macrocephaly. Individual 9 had bilateral
619 epileptiform discharges on EEG, autistic features, DD, and ID. Individual 11 had autism, DD,
620 and ID. Our amino acid conservation analysis showed that affected residues in the PPFIA3
621 coiled-coil domain are highly conserved, except for the residues p.Glu40 and p.Arg498, across
622 mice, fruit flies, and C. elegans (**Figure S1A, B**). These findings suggest the affected residues
623 are critical for the protein's function across different species. Furthermore, molecular modeling
624 of p.(Arg415Trp) and p.(Arg429Trp) variants suggested that the missense variants would hinder
625 PPFIA3 function.
626
627 Three individuals have *de novo PPFIA3* missense variants (12, p.(Trp546Cys); 13,
628 p.(Arg784Trp); and 17, p.(Ser906Leu)) in the intrinsically disordered region of the protein. The
629 amino acid conservation analysis suggests that the affected residues are not well-conserved
630 across species, except for p.Ser906 that is near the SAM1 domain. Individual 12 had autism,
631 DD, and ID, whereas individual 13 had epilepsy, DD, and ID. Individual 17 (p.(Ser906Leu)) had
632 abnormal EEG, autism, DD, ID, hypotonia, dysmorphisms, and micro/macrocephaly. Together,
633 these findings suggest that variants in the intrinsically disordered regions are associated with
634 variable disease severity, which may be due to the lack of association in this region with
635 functional domains for PPFIA3. Two monozygotic twins had *PPFIA3* missense variants in the
636 SAM1 domain (14 and 15, p.(Ile870Asn)). Individual 14 had autism, DD, ID, and microcephaly
637 and individual 15 had DD, ID, hypotonia, and microcephaly. Individual 18 has a *PPFIA3*
638 frameshift variant in the SAM3 domain, p.(Glu1103Asnfs*8), with abnormal EEG, DD, ID,
639 hypotonia, and dysmorphisms. There were two related individuals (5 and 6) with a *PPFIA3*
640 intronic splice variant (c.240+1G>A) and DD, ID, dysmorphisms, and microcephaly. Individual 5

641 inherited the *PPFIA3* variant from the affected parent, individual 6. The inheritance of the
642 *PPFIA3* variant in individual 6 is unknown. One individual (20) was identified with compound
643 heterozygous variants, p.(Pro793Thr) and p.(Lys759Arg), which were inherited from
644 asymptomatic parents. This individual has DD, ID, epilepsy, autistic features, hypotonia,
645 dysmorphism, and microcephaly. As this is the only individual with biallelic variants in *PPFIA3*
646 described to date in GeneMatcher[38–40], the significance of these variants is uncertain until
647 additional individuals with similar features and biallelic *PPFIA3* variants are identified. However,
648 there are striking similarities in facial features and clinical phenotypes between individual 20 and
649 other individuals in the cohort. Finally, we also identified a rare missense *PPFIA3* p.(Arg559Trp)
650 (NM_003660.4:c.1675C>T) variant of unknown inheritance in an individual with a discordant
651 severe neurodegeneration phenotype and family history of consanguinity (data not shown). This
652 variant is not present in gnomAD v2.1.1 and has a CADD (v1.6) score of 24.6, suggesting this
653 variant could be potentially damaging. However, the severe neurodegeneration phenotype was
654 not observed in the 20 individuals in our cohort. This suggests that *PPFIA3* p.(Arg559Trp) is
655 either a more severe deleterious variant or there are other genetic alterations, including
656 alterations that may be related to the family history of consanguinity, contributing to this
657 individual's clinical findings.
658
659 Our conservation analysis revealed that the PPFIA3 domains are well-conserved in the fruit fly
660 homolog, Liprin-α, which is primarily found in the fruit fly embryonic and larval nervous system.
661 We utilized the evolutionary conservation to assess the impact of *PPFIA3* variants on
662 development and behavior in the fruit fly. We found that ubiquitous expression of *PPFIA3*
663 missense variants in the coiled-coil domain (p.(Arg39Cys), p.(Ala315Ser), and p.(Arg415Trp))
664 resulted in pupal lethality and or eclosion defects. Interestingly, p.(Arg39Cys) caused severe
665 pupal lethality, whereas p.(Ala315Ser) and p.(Arg415Trp) had milder effects on pupal lethality.
666 All three tested variants in the coiled-coil domain showed abnormal leg morphology. Neuron-
667 specific expression of *PPFIA3* p.(Arg39Cys) and p.(Arg415Trp) variants showed bang sensitivity
668 and climbing defects. Furthermore, as *Liprin-α* is known to regulate NMJ development in fruit
669 flies, we examined the effect of human *PPFIA3* WT and variant cDNA expression in the larval
670 NMJ. We found that *PPFIA3* p.(Arg39Cys) and p.(Arg415Trp) caused a reduction in bouton
671 number compared to *PPFIA3* WT, which would potentially impair neurotransmission. Our fly
672 overexpression findings reveal the *PPFIA3* missense variants in the coiled-coil domain cause
673 lethality, suggesting these variants are dominant negative alleles. Interestingly, ubiquitous, or
674 neuronal overexpression of the *PPFIA3* variants in the intrinsically disordered region

675 (p.(Arg784Trp) and p.(Trp546Cys)) had either mild or no phenotypes in the fruit flies, which may
676 be due to the variants are either not conserved in the flies, cause mild protein dysfunction that is
677 tolerated in the fly model, or these variants are benign and the phenotypes are due to other
678 genetic etiologies. However, knowledge regarding the presence of Liprin-α outside the nervous
679 system during Drosophila postembryonic development is limited.[49] Therefore, the genetic
680 mechanism underlying the *PPFIA3* variants associated phenotypes in the fruit flies may be more
681 complex.
682
683 To further determine whether the variants are LOF or gain-of-function (GOF) in nature and the
684 functional conservation between human *PPFIA3* and fly *Liprin-α*, we performed a LOF lethality
685 rescue assay using *Liprin-α* mutants and *PPFIA3* WT and variants. Our LOF rescue assay
686 showed that human *PPFIA3* WT partially rescued the *Liprin-α* LOF embryonic lethality and
687 development to the adult stage, suggesting that human PPFIA3 WT function is partially
688 conserved in fruit flies. Interestingly, the coiled-coil variants, *PPFIA3* p.(Arg39Cys) and
689 p.(Arg415Trp), showed reduced rescue efficiency of the *Liprin-α* LOF embryonic lethality,
690 indicating these variants are strong LOF variants. In contrast, the intrinsically disordered region
691 variants, *PPFIA3* p.(Trp546Cys) and p.(Arg784Trp), showed a similar rescue efficiency of the
692 embryonic lethality as compared to *PPFIA*3 WT. However, we found in the adult stage that
693 *PPFIA3* p.(Arg784Trp) significantly reduced the lifespan of rescue flies compared to *PPFIA3*
694 WT, suggesting that p.(Arg784Trp) is a hypomorphic LOF variant. These findings are consistent
695 with the clinical findings in individuals 11, p.(Trp546Cys) and 12, p.(Arg784Trp). Both individuals
696 had fewer clinical features reported. In contrast, individuals 1 and 2, p.(Arg39Cys) and
697 individuals 8 and 9, p.(Arg415Trp) had more clinical features reported. Together, our
698 overexpression and LOF rescue assays in fruit flies reveal that rare *PPFIA3* variants cause a
699 neurodevelopmental disorder through a LOF mechanism and suggest that disease severity
700 correlates with the degree of LOF.
701
702 Together, the clinical phenotypes and functional assays in fruit flies point towards a possible
703 domain-specific disease severity mechanism where the variants in the coiled-coil domains might
704 lead to relatively more severe phenotypes in both affected individuals and fruit flies. Notably, ten
705 individuals in the cohort have a family history of neurologic findings, which include ID, autism,
706 NDD, dyslexia, muscular dystrophy, and psychiatric illnesses (**Tables S4 and S5, see**
707 **Supplemental Note**). These familial findings raise the possibility that genetic background
708 effects may also contribute to the severity and penetrance of *PPFIA3*-related phenotypes.

709 However, the current number of participants and tested variants limits the prediction of
710 genotype-phenotype correlations. Further studies in a larger sample size of affected individuals
711 will be required to elucidate potential genotype-phenotype correlations.
712
713 Finally, to determine if *PPFIA3* copy number variants (CNVs) may potentially be contributory to
714 neurodevelopmental phenotypes, we examined CNVs involving the *PPFIA3* locus in DECIPHER
715 v11.21, gnomAD SVs v2.1, and ClinVar.[37,50,51] Across all three databases, seven individuals
716 were reported with *PPFIA3* CNV deletions, but phenotypic information is limited to one
717 individual reported with autistic behavior and mild microcephaly and one individual reported with
718 a progressive familial heart block type IB (**Figure S8A, Table S8**). There are 82 individuals
719 reported with chromosomal duplications in these databases (**Figure S8A, Table S8**). However,
720 in gnomAD SV 2.1 there were three individuals found to be homozygous and 38 individuals
721 found to be heterozygous for a 42.9 kb duplication involving both the *PPFIA3* and *TRPM4* loci
722 (**Table S8**), suggesting that *PPFIA3* duplication may be tolerated. Altogether, the phenotypes
723 associated with the reported CNV deletions and duplications involving the *PPFIA3* locus include
724 DD, ID, seizures, dysmorphisms, autistic behavior, microcephaly, and behavioral abnormalities
725 (**Figure S8**, **Table S8**). Together, these findings suggest that *PPFIA3* deletions may contribute
726 to the pathogenesis of neurodevelopmental disorders, but further studies will be needed to
727 determine the significance of *PPFIA3* haploinsufficiency in human disease.
728
729 In summary, our study provides clinical and functional evidence that rare *PPFIA3* variants cause
730 a syndromic neurodevelopmental disorder characterized by DD, ID, hypotonia, ASD or autistic
731 features, dysmorphisms, and epilepsy. The reduced penetrance of features in affected family
732 members suggests a complex relationship between *PPFIA3* germline variants and
733 developmental features. Together, our *in vivo* functional modeling in fruit flies reveal that
734 *PPFIA3* variants may contribute to disease pathogenesis through LOF mechanisms related to
735 the location of the affected residues in the PPFIA3 functional domains. These findings and our
736 clinical characterizations show that rare *PPFIA3* variants lead to a syndromic
737 neurodevelopmental disorder. Future approaches to further elucidate the mechanistic
738 underpinnings of *PPFIA3* variants in disease pathogenesis may include synaptic ultrastructural
739 analysis with transmission electron microscopy, electrophysiology to analyze the synaptic
740 recycling system, and genotype to phenotype correlations with fruit fly functional assays for the
741 17 identified *PPFIA3* variants. Longitudinal assessments in a larger sample size of affected
742 individuals and mechanistic studies in model organisms will advance our understanding of

743 disease pathogenesis, improve prognostication based on variant type and location, and identify
744 potential therapeutic avenues.
745
746 **DECLARATION OF INTERESTS**
747 The Department of Molecular and Human Genetics at Baylor College of Medicine derives
748 revenue from the clinical exome sequencing services offered at Baylor Genetics. JLM, MJGS,
749 and RP are employees of GeneDx, LLC.
750
751 **CONSORTIA**
752 **Members of the Undiagnosed Diseases Network (UDN):** Maria T. Acosta, Margaret Adam,
753 David R. Adams, Raquel L. Alvarez, Justin Alvey, Laura Amendola, Ashley Andrews, Euan A.
754 Ashley, Carlos A. Bacino, Guney Bademci, Ashok Balasubramanyam, Dustin Baldridge, Jim
755 Bale, Michael Bamshad, Deborah Barbouth, Pinar Bayrak-Toydemir, Anita Beck, Alan H.
756 Beggs, Edward Behrens, Gill Bejerano, Hugo J. Bellen, Jimmy Bennett, Beverly Berg-Rood,
757 Jonathan A. Bernstein, Gerard T. Berry, Anna Bican, Stephanie Bivona, Elizabeth Blue, John
758 Bohnsack, Devon Bonner, Lorenzo Botto, Brenna Boyd, Lauren C. Briere, Gabrielle Brown,
759 Elizabeth A. Burke, Lindsay C. Burrage, Manish J. Butte, Peter Byers, William E. Byrd, John
760 Carey, Olveen Carrasquillo, Thomas Cassini, Ta Chen Peter Chang, Sirisak Chanprasert,
761 Hsiao-Tuan Chao, Ivan Chinn, Gary D. Clark, Terra R. Coakley, Laurel A. Cobban, Joy D.
762 Cogan, Matthew Coggins, F. Sessions Cole, Heather A. Colley, Heidi Cope, Rosario Corona,
763 William J. Craigen, Andrew B. Crouse, Michael Cunningham, Precilla D'Souza, Hongzheng Dai,
764 Surendra Dasari, Joie Davis, Jyoti G. Dayal, Esteban C. Dell'Angelica, Katrina Dipple, Daniel
765 Doherty, Naghmeh Dorrani, Argenia L. Doss, Emilie D. Douine, Dawn Earl, David J. Eckstein,
766 Lisa T. Emrick, Christine M. Eng, Marni Falk, Elizabeth L. Fieg, Paul G. Fisher, Brent L. Fogel,
767 Irman Forghani, William A. Gahl, Ian Glass, Bernadette Gochuico, Page C. Goddard, Rena A.
768 Godfrey, Katie Golden-Grant, Alana Grajewski, Don Hadley, Sihoun Hahn, Meghan C. Halley,
769 Rizwan Hamid, Kelly Hassey, Nichole Hayes, Frances High, Anne Hing, Fuki M. Hisama, Ingrid
770 A. Holm, Jason Hom, Martha Horike-Pyne, Alden Huang, Sarah Hutchison, Wendy Introne,
771 Rosario Isasi, Kosuke Izumi, Fariha Jamal, Gail P. Jarvik, Jeffrey Jarvik, Suman Jayadev, Orpa
772 Jean-Marie, Vaidehi Jobanputra, Lefkothea Karaviti, Shamika Ketkar, Dana Kiley, Gonench
773 Kilich, Shilpa N. Kobren, Isaac S. Kohane, Jennefer N. Kohler, Susan Korrick, Mary Kozuira,
774 Deborah Krakow, Donna M. Krasnewich, Elijah Kravets, Seema R. Lalani, Byron Lam, Christina
775 Lam, Brendan C. Lanpher, Ian R. Lanza, Kimberly LeBlanc, Brendan H. Lee, Roy Levitt,
776 Richard A. Lewis, Pengfei Liu, Xue Zhong Liu, Nicola Longo, Sandra K. Loo, Joseph Loscalzo,

Richard L. Maas, Ellen F. Macnamara, Calum A. MacRae, Valerie V. Maduro, Audrey Stephannie Maghiro, Rachel Mahoney, May Christine V. Malicdan, Laura A. Mamounas, Teri A. Manolio, Rong Mao, Kenneth Maravilla, Ronit Marom, Gabor Marth, Beth A. Martin, Martin G. Martin, Julian A. Martínez-Agosto, Shruti Marwaha, Jacob McCauley, Allyn McConkie-Rosell, Alexa T. McCray, Elisabeth McGee, Heather Mefford, J. Lawrence Merritt, Matthew Might, Ghayda Mirzaa, Eva Morava, Paolo Moretti, John Mulvihill, Mariko Nakano-Okuno, Stanley F. Nelson, John H. Newman, Sarah K. Nicholas, Deborah Nickerson, Shirley Nieves-Rodriguez, Donna Novacic, Devin Oglesbee, James P. Orengo, Laura Pace, Stephen Pak, J. Carl Pallais, Christina G.S. Palmer, Jeanette C. Papp, Neil H. Parker, John A. Phillips III, Jennifer E. Posey, Lorraine Potocki, Barbara N. Pusey Swerdzewski, Aaron Quinlan, Deepak A. Rao, Anna Raper, Wendy Raskind, Genecee Renteria, Chloe M. Reuter, Lynette Rives, Amy K. Robertson, Lance H. Rodan, Jill A. Rosenfeld, Natalie Rosenwasser, Francis Rossignol, Maura Ruzhnikov, Ralph Sacco, Jacinda B. Sampson, Mario Saporta, Judy Schaechter, Timothy Schedl, Kelly Schoch, Daryl A. Scott, C. Ron Scott, Elaine Seto, Vandana Shashi, Jimann Shin, Edwin K. Silverman, Janet S. Sinsheimer, Kathy Sisco, Edward C. Smith, Kevin S. Smith, Lilianna Solnica-Krezel, Ben Solomon, Rebecca C. Spillmann, Joan M. Stoler, Kathleen Sullivan, Jennifer A. Sullivan, Angela Sun, Shirley Sutton, David A. Sweetser, Virginia Sybert, Holly K. Tabor, Queenie K.-G. Tan, Amelia L. M. Tan, Arjun Tarakad, Mustafa Tekin, Fred Telischi, Willa Thorson, Cynthia J. Tifft, Camilo Toro, Alyssa A. Tran, Rachel A. Ungar, Tiina K. Urv, Adeline Vanderver, Matt Velinder, Dave Viskochil, Tiphanie P. Vogel, Colleen E. Wahl, Melissa Walker, Stephanie Wallace, Nicole M. Walley, Jennifer Wambach, Jijun Wan, Lee-kai Wang, Michael F. Wangler, Patricia A. Ward, Daniel Wegner, Monika Weisz Hubshman, Mark Wener, Tara Wenger, Monte Westerfield, Matthew T. Wheeler, Jordan Whitlock, Lynne A. Wolfe, Kim Worley, Changrui Xiao, Shinya Yamamoto, John Yang, Zhe Zhang, Stephan Zuchner

ACKNOWLEDGEMENTS

We thank the families and clinical staff at each location for participation in this study. In addition, we thank Mingshan Xue, Dongwon Lee, Kailin Mao, Wu (Charles) Chen, Brooke Horist, and Cole Deisseroth for critical feedback on the manuscript. H.T.C.'s research work is supported by the McNair Medical Institute at The Robert and Janice McNair Foundation, the Burroughs Wellcome Fund, Child Neurology Foundation and Society, The Gordan and Mary Cain Foundation, Annie and Bob Graham, The Elkins Foundation, and the Mark A. Wallace Endowment Award. M.S.P.'s research effort is supported in part by the National Ataxia Foundation and the Burroughs Wellcome Fund. J.M.P.'s research effort was supported in part

811 by the Burroughs Wellcome Fund. V.C.L and S.L.M. were supported in part by The Gordan and
812 Mary Cain Foundation and Annie and Bob Graham. S.L.M. was also supported in part by the
813 Mark A. Wallace Endowment Award. This work was also supported by Texas Children's
814 Hospital, the Jan and Dan Duncan Neurological Research Institute, and the Eunice Kennedy
815 Shriver National Institute of Child Health & Human Development of the National Institutes of
816 Health under Award Number P50HD103555 for use of the Clinical Translational Core and
817 Microscopy Core facilities. Research reported in this manuscript was supported by the NIH
818 Common Fund, through the Office of Strategic Coordination/Office of the NIH Director under
819 Award Number - U01HG007709. The content is solely the responsibility of the authors and does
820 not necessarily represent the official views of the National Institutes of Health.
821

822 **AUTHOR CONTRIBUTIONS**

823 M.S.P. and H.T.C. contributed to the conception and design of the study, the acquisition and
824 analysis of data, drafting the text, and preparing figures and tables. S.L.M., H.P., V.C.L., A.T.,
825 M.A.L., M.W-H., R.A.L., MR.B., N.B., L.M., S.P., J.T., J.L.M., S.R.C., L.L., T.P., D.Z., L.F., S.M.,
826 G.V.,S.R-H., G.L.C., C.A.B., B.H.L., H.Y.K., A.P., J.B., C.P., D.S.J.S., A.M., M.B.T., E.G.K.,
827 R.M., G.B.S., V.R., P.V.,C.P., and M.O. contributed to the acquisition and analysis of data.
828 J.M.P. and H.C. contributed to analysis of data and preparing figures. J.A.R., M.Z., M.W., H.E.,
829 K.C., E.M., M.J.G-S., R.P., P.P.M., A.S.A.C., J-B.LP., K.E., C.R., A-S.D-P., S.S., I.E.S., H.M.
830 contributed to the acquisition and analysis of data, drafting the text, and preparing tables.
831

832 **WEB RESOURCES**

833 CADD, https://cadd.gs.washington.edu/
834 ClinVAR, https://www.ncbi.nlm.nih.gov/clinvar/
835 CLUSTAL Omega, https://www.ebi.ac.uk/Tools/msa/clustalo/
836 Decipher, https://www.deciphergenomics.org/
837 DIOPT, https://fgr.hms.harvard.edu/diopt
838 GeneMatcher, https://genematcher.org/
839 gnomAD, https://gnomad.broadinstitute.org/
840 ImageJ, https://github.com/imagej/ImageJ
841 Imaris, https://imaris.oxinst.com/
842 MCAP, http://bejerano.stanford.edu/mcap/
843 OMIM, https://www.omim.org/
844 PyMOL, https://pymol.org/2/

845 SIFT, https://sift.bii.a-star.edu.sg/www/Extended_SIFT_chr_coords_submit.html
846 UCSC genome browser, https://genome.ucsc.edu/
847
848 **DATA AND CODE AVAILABILITY**
849 The de-identified data supporting the current study are available from the corresponding author
850 on request. The submission and accession numbers for the variants reported to ClinVar are (1)
851 Individuals 1 and 2, ClinVar: SCV003804191.1; GenBank:NM_003660.4 (PPFIA3); c.115 C>T
852 (p.Arg39Cys); (2) Individual 4, ClinVar: SCV003804194.1; c.239 A>C (p.Gln80Pro); (3)
853 Individuals 8 and 9, ClinVar: SCV003804192.1; c.1243 C>T (p.Arg415Trp); (4) Individual 10,
854 ClinVar: SCV003801340; c.1285C>T (p.Arg429Trp); (5) Individual 11, ClinVar: SCV003840201;
855 c.1492 C>T (p.Arg498Trp); (6) Individual 12, ClinVar: SCV003804193.1; c.1638 G>T
856 (p.Trp546Cys); (7) Individual 13, ClinVar: SCV003801341; c.2350 C>T (p.Arg784Trp); (8)
857 Individuals 14 and 15, ClinVar: SCV004042691.1; c.2609T>A (p.Ile870Asn); (9) Individual 17,
858 ClinVar: SCV003035511; c.2717 C>T (p.Ser906Leu); (10) Individual 18, ClinVar:
859 SCV003035512; c.3307del (p.Glu1103Asnfs*8).
860
861 The following variants have been submitted to the ClinVar and the data are scheduled to be
862 released publicly between April 10, 2024 to April 29, 2024: (1) Individual 3, ClinVar:
863 SCV004041597; c.118G>A (p.Glu40Lys); (2) Individuals 5 and 6, ClinVar: SCV004041598;
864 c.240+1G>A; (3) Individual 7, ClinVar: SCV004041599; c.943 G>T; (p.Ala315Ser); (4) Individual
865 16, ClinVar: SCV004171207; c.2706dup; p.(Ser903Leufs*86); (5) Individual 19, ClinVar:
866 SCV004041600; deletion exons 22-30; (6) Individual 20, ClinVar: SCV004041615; c.2377C>A;
867 (p.Lys759Arg) (7) Individual 20, ClinVar: SCV004041614; c.2276 A>G; (p.Pro793Thr).
868
869 **SUPPLEMENTAL MATERIAL**
870 Supplementary material includes eight tables and eight figures.
871
872

873 **FIGURE LEGENDS**

874 **Figure 1: Variant location and images of individuals with PPFIA3 variants (A)** Location of
875 *PPFIA3* variants in the genomic locus corresponding to the exon-intron structure. Number of
876 individuals with the rare *PPFIA3* variant shown in the y-axis. **(B)** Location of *PPFIA3* variants in
877 the corresponding protein domains. Number of individuals with the variant shown in the y-axis.
878 The fruit fly homolog, *Liprin-α*, shows 48% identity and 62% similarity with the human *PPFIA3*.
879 Sterile alpha motif (SAM). **(C)** Images of individuals with heterozygous or compound
880 heterozygous *PPFIA3* variants. The three individuals shown have dysmorphic features such as
881 wide mouth, widely spaced teeth, prominent forehead, and hypotonic facies.

882

883 **Figure 2: Molecular modeling of *PPFIA3* missense variants and protein levels in PPFIA3**
884 **variants. (A and B)** PPFIA3 missense variants are modeled in PyMol (version 2.5.2) with
885 GenBank NP_003651.1. Human PPFIA3 WT residues are modeled in gray with coiled coils
886 displayed in black and affected residues are highlighted in orange. Local polar contacts (orange
887 dashed lines) and residue interactions (highlighted in pink) are displayed before and after
888 mutagenesis for **(Bi)** p.(Arg415Trp), **(Bii)** p.(Arg429Trp), **(Ci)** p.(Arg784Trp), **(Cii)**
889 p.(Ser906Leu). **(C) (i)** Western blot from PPFIA3 WT and variants show higher levels of HA in
890 PPFIA3 p.(Arg39Cys) compared to WT. **(ii)** Quantification of relative HA in 4-6 sets of biological
891 replicates show higher level of HA in PPFIA3 p.(Arg39Cys) producing flies. Statistical analysis
892 conducted with one-way ANOVA and Tukey's post-hoc analysis. Data shown as mean ± SEM.
893 Significance shown as $***p<0.001$. Non-significance shown as ns.

894

895 **Figure 3: *Actin-GAL4* mediated ubiquitous expression of *PPFIA3* variants cause**
896 **developmental and anatomical defects in fruit flies. (A)** Pupal lethality and eclosion defect
897 associated with *Actin-GAL4* mediated overexpression of *PPFIA3* variants. **(i)** Images showing
898 overexpression of *PPFIA3* p.(Arg39Cys) cause pupal lethality and eclosion defect, and

899 p.(Ala315Ser) and p.(Arg415Trp) cause eclosion defect compared to the *PPFIA3* WT and *UAS*-
900 empty control. Uneclosed flies from p.(Arg39Cys), p.(Ala315Ser), and p.(Arg415Trp) remain in
901 the pupal case. *PPFIA3* p.(Trp546Cys) and p.(Arg784Trp) overexpression does not cause a
902 difference in pupal lethality and eclosion defect compared to *PPFIA3* WT and *UAS*-empty
903 control flies. Scale bar = 100 μm. **(ii)** Bar graphs showing the percentage of eclosed pupae
904 (overexpression), eclosion defect, and pupal lethal. Statistical analysis conducted with one-way
905 ANOVA and Tukey's post-hoc analysis. Data shown as mean ± SEM with the sample size of
906 total number of pupae in three sets. Significance shown as $**p<0.01$ and $***p<0.001$. Non-
907 significance shown as ns. **(B)** Images of leg morphology associated with *Actin-GAL4*-mediated
908 overexpression of *PPFIA3* variants. **(i)** Empty control and PPFIA3 WT expressing flies have
909 typical legs with three segments. *PPFIA3* p.(Arg39Cys), p.(Ala315Ser), and p.(Arg415Trp) result
910 in pronounced leg segment developmental defects compared to *PPFIA3* WT. Mild leg
911 segmental developmental defects found with *PPFIA3* p.(Arg784Trp) but not significant
912 compared to *PPFIA3* WT. No leg defects were found in *PPFIA3* p.(Trp546Cys) flies. Scale bar =
913 100 μm. **(ii)** Bar graph showing the percentage of flies with abnormal leg morphology. Statistical
914 analysis conducted with one-way ANOVA and Tukey's post-hoc analysis. Data shown as mean
915 ± SEM with the sample size of total number of adult flies in three sets. Significance shown as
916 $***p<0.001$. Non-significance shown as ns.
917
918 **Figure 4: *elav-GAL4* mediated neuronal overexpression of *PPFIA3* variants result in**
919 **climbing defect, bang sensitivity, and neuromuscular junction (NMJ) bouton loss. (A)**
920 *elav-GAL4* mediated neuronal expression of *PPFIA3* p.(Arg39Cys), *PPFIA3* p.(Ala315Ser),
921 *PPFIA3* p.(Arg415Trp), and *PPFIA3* p.(Arg784Trp) result in impaired motor coordination on the
922 climbing assay compared to *PPFIA3* WT and empty control flies. Crosses were set and
923 maintained at 25ºC. Behavioral testing was conducted at 20-21ºC with both sexes. **(B)** *elav-*

924 *GAL4* mediated neuronal expression of *PPFIA3* p.(Arg39Cys), *PPFIA3* p.(Ala315Ser), and
925 *PPFIA3* p.(Arg415Trp) have bang sensitivity with delayed recovery from vortexing compared to
926 *PPFIA3* WT and *UAS*-empty control flies. Crosses were set and maintained at 25°C. Behavioral
927 test was conducted at 20-21°C with both sexes. **(C)** *elav-GAL4* mediated neuronal
928 overexpression of *PPFIA3* variants result in NMJ bouton loss without a significant change in
929 NMJ length. **(i)** Model depicting the method for visualizing the NMJ in fruit fly 3rd instar larva. **(ii)**
930 Representative images of 3rd instar larval NMJs of each genotype including *elav GAL4>UAS*
931 empty, *elav GAL4>PPFIA3* WT, p.(Arg39Cys), p.(Arg415Trp), p.(Trp546Cys), and
932 p.(Arg784Trp) are shown. HRP (Horseradish Peroxidase) is a pan-neuronal marker (green) and
933 Brp (Bruchpilot) is an active zone marker (magenta). Scale bar is 24 μm. **(iii)** Quantification of
934 total number of boutons in the muscle 6/7 (abdominal segment A3) NMJ show that *PPFIA3*
935 p.(Arg39Cys) and p.(Arg415Trp) result in bouton loss compared to *PPFIA3* WT and empty
936 control. In contrast, *PPFIA3* p.(Trp546Cys) and p.(Arg784Trp) show no alteration in bouton
937 numbers. **(iv)** Quantification of total NMJ length in each genotype is shown and there is no
938 significant difference between *PPFIA3* WT, variants, and *UAS*-empty control. Crosses were set
939 and maintained at 25°C. Statistical analysis conducted with one-way ANOVA and Tukey's post-
940 hoc analysis. Data shown as mean ± SEM with the sample size of total number of quantified
941 NMJs shown in the bars. Significance shown as $**p<0.01$, $***p<0.001$. Non-significance shown
942 as ns.
943
944 **Figure 5: PPFIA3 WT partially rescues the fly Liprin-α LOF lethality. (A)** Human PPFIA3
945 WT in the background of fly Liprin-α LOF results in a partial rescue of embryonic lethality. **(i)**
946 Crossing-scheme to delete fly *Liprin-α* and express human *PPFIA3* WT and variants. The
947 scheme describes the rescue larvae selection strategy. Crosses were set and maintained at
948 20°C. **(ii)** Quantification of n = 3 sets per genotype showing % GFP-negative larvae (rescue

949 larvae) that survive to the larval stage. *PPFIA3* WT expression can partially rescue larval
950 viability compared to empty control. *PPFIA3* p.(Arg39Cys) and p.(Arg415Trp) show impaired
951 ability to rescue larval viability. **(B)** Human *PPFIA3* WT expression partially rescues the lethality
952 in adult stage. **(i)** Representative illustration of the different stages of fruit fly development. **(ii)**
953 Quantification of 3 sets of rescued larvae per genotype that survive to the adult stage. *PPFIA3*
954 WT expression can partially rescue adult viability compared to empty control. *PPFIA3*
955 p.(Arg39Cys) and p.(Arg415Trp) show impaired ability to rescue adult viability. **(iii)**
956 Quantification of 1-3 sets of rescued larvae per genotype that survived after 48 hours post-
957 eclosion. For the empty control larvae only one escaper rescue larvae survived to adult stage
958 but died within 2 days post-eclosion. None of the *PPFIA3* p.(Arg39Cys) rescue larvae survived
959 to adult stage. Due to the lack of any *PPFIA3* p.(Arg39Cys) rescue larvae surviving to the adult
960 stage, this variant was not quantifiable for the adult survival phenotype. *PPFIA3* p.(Arg415Trp)
961 and *PPFIA3* p.(Arg784Trp) show impaired ability to rescue adult viability compared to the
962 *PPFIA3* WT. Sample size is shown in Table S2. Statistical analysis with one-way ANOVA and
963 Tukey's post-hoc analysis. Data shown as mean ± SEM with the sample size of flies scored
964 shown in **(Table S2)**. Significance shown as $*p<0.05$, $**p<0.01$, $***p<0.001$. Non-significance
965 shown as ns.
966
967 **TABLES**
968 **Table 1: Genetic and neurologic findings in individuals with rare *PPFIA3* variants and**
969 **neurodevelopmental phenotypes**
970
971 **Table 2: In silico predictions for *PPFIA3* variants (individuals 1-20)**
972
973 **Table 3: Comparison of clinical phenotypes and findings in fruit flies expressing *PPFIA3***
974 **missense variants**
975

976 **REFERENCES**

977 1. Südhof, T.C. (2013). Neurotransmitter Release: The Last Millisecond in the Life of a
978 Synaptic Vesicle. Neuron *80*, 675–690. 10.1016/j.neuron.2013.10.022.

979 2. Südhof, T.C. (2004). The synaptic vesicle cycle. Annu. Rev. Neurosci. *27*, 509–547.
980 10.1146/annurev.neuro.26.041002.131412.

981 3. Zhai, R.G., and Bellen, H.J. (2004). The Architecture of the Active Zone in the Presynaptic
982 Nerve Terminal. Physiology *19*, 262–270. 10.1152/physiol.00014.2004.

983 4. Xue, M., Giagtzoglou, N., and Bellen, H.J. (2011). Dueling Ca2+ Sensors in
984 Neurotransmitter Release. Cell *147*, 491–493. 10.1016/j.cell.2011.10.007.

985 5. Südhof, T.C. (2012). The Presynaptic Active Zone. Neuron *75*, 11–25.
986 10.1016/j.neuron.2012.06.012.

987 6. Hoischen, A., Krumm, N., and Eichler, E.E. (2014). Prioritization of neurodevelopmental
988 disease genes by discovery of new mutations. Nat Neurosci *17*, 764–772. 10.1038/nn.3703.

989 7. Mencacci, N.E., Brockmann, M.M., Dai, J., Pajusalu, S., Atasu, B., Campos, J., Pino, G.,
990 Gonzalez-Latapi, P., Patzke, C., Schwake, M., et al. (2021). Biallelic variants in TSPOAP1,
991 encoding the active-zone protein RIMBP1, cause autosomal recessive dystonia. Journal of
992 Clinical Investigation *131*, e140625. 10.1172/JCI140625.

993 8. Lepeta, K., Lourenco, M.V., Schweitzer, B.C., Martino Adami, P.V., Banerjee, P., Catuara-
994 Solarz, S., de La Fuente Revenga, M., Guillem, A.M., Haidar, M., Ijomone, O.M., et al.
995 (2016). Synaptopathies: synaptic dysfunction in neurological disorders - A review from
996 students to students. J. Neurochem. *138*, 785–805. 10.1111/jnc.13713.

997 9. Taoufik, E., Kouroupi, G., Zygogianni, O., and Matsas, R. (2018). Synaptic dysfunction in
998 neurodegenerative and neurodevelopmental diseases: an overview of induced pluripotent
999 stem-cell-based disease models. Open Biol. *8*, 180138. 10.1098/rsob.180138.

1000 10. Chen, W., Cai, Z.-L., Chao, E.S., Chen, H., Longley, C.M., Hao, S., Chao, H.-T., Kim, J.H.,
1001 Messier, J.E., Zoghbi, H.Y., et al. (2020). Stxbp1/Munc18-1 haploinsufficiency impairs
1002 inhibition and mediates key neurological features of STXBP1 encephalopathy. eLife *9*,
1003 e48705. 10.7554/eLife.48705.

1004 11. Serra-Pagès, C., Kedersha, N.L., Fazikas, L., Medley, Q., Debant, A., and Streuli, M.
1005 (1995). The LAR transmembrane protein tyrosine phosphatase and a coiled-coil LAR-
1006 interacting protein co-localize at focal adhesions. The EMBO Journal *14*, 2827–2838.
1007 10.1002/j.1460-2075.1995.tb07282.x.

1008 12. Serra-Pagès, C., Medley, Q.G., Tang, M., Hart, A., and Streuli, M. (1998). Liprins, a Family
1009 of LAR Transmembrane Protein-tyrosine Phosphatase-interacting Proteins. Journal of
1010 Biological Chemistry *273*, 15611–15620. 10.1074/jbc.273.25.15611.

1011 13. Taru, H., and Jin, Y. (2011). The Liprin Homology Domain Is Essential for the Homomeric
1012 Interaction of SYD-2/Liprin-α Protein in Presynaptic Assembly. J. Neurosci. *31*, 16261–
1013 16268. 10.1523/JNEUROSCI.0002-11.2011.

1014 14. Schoch, S., Castillo, P.E., Jo, T., Mukherjee, K., Geppert, M., Wang, Y., Schmitz, F.,
1015 Malenka, R.C., and Südhof, T.C. (2002). RIM1α forms a protein scaffold for regulating
1016 neurotransmitter release at the active zone. Nature *415*, 321–326. 10.1038/415321a.

1017 15. Ko, J., Na, M., Kim, S., Lee, J.-R., and Kim, E. (2003). Interaction of the ERC Family of RIM-
1018 binding Proteins with the Liprin-α Family of Multidomain Proteins. Journal of Biological
1019 Chemistry *278*, 42377–42385. 10.1074/jbc.M307561200.

1020 16. Dai, Y., Taru, H., Deken, S.L., Grill, B., Ackley, B., Nonet, M.L., and Jin, Y. (2006). SYD-2
1021 Liprin-α organizes presynaptic active zone formation through ELKS. Nat Neurosci *9*, 1479–
1022 1487. 10.1038/nn1808.

1023 17. Kim, C. (2003). SAM domains: uniform structure, diversity of function. Trends in Biochemical
1024 Sciences *28*, 625–628. 10.1016/j.tibs.2003.11.001.

1025 18. Pulido, R., Serra-Pagès, C., Tang, M., and Streuli, M. (1995). The LAR/PTP delta/PTP
1026 sigma subfamily of transmembrane protein-tyrosine-phosphatases: multiple human LAR,
1027 PTP delta, and PTP sigma isoforms are expressed in a tissue-specific manner and
1028 associate with the LAR-interacting protein LIP.1. Proc. Natl. Acad. Sci. U.S.A. *92*, 11686–
1029 11690. 10.1073/pnas.92.25.11686.

1030 19. Van Der Lee, R., Buljan, M., Lang, B., Weatheritt, R.J., Daughdrill, G.W., Dunker, A.K.,
1031 Fuxreiter, M., Gough, J., Gsponer, J., Jones, D.T., et al. (2014). Classification of Intrinsically
1032 Disordered Regions and Proteins. Chem. Rev. *114*, 6589–6631. 10.1021/cr400525m.

1033 20. Babu, M.M. (2016). The contribution of intrinsically disordered regions to protein function,
1034 cellular complexity, and human disease. Biochemical Society Transactions *44*, 1185–1200.
1035 10.1042/BST20160172.

1036 21. Liu, Y.C., Couzens, A.L., Deshwar, A.R., McBroom-Cerajewski, L.D.B., Zhang, X.,
1037 Puviindran, V., Scott, I.C., Gingras, A.C., Hui, C.C., and Angers, S. (2014). The PPFIA1-
1038 PP2A protein complex promotes trafficking of Kif7 to the ciliary tip and Hedgehog signaling.
1039 Science Signaling *7*, 1–13. 10.1126/scisignal.2005608.

1040 22. van der Vaart, B., van Riel, W.E., Doodhi, H., Kevenaar, J.T., Katrukha, E.A., Gumy, L.,
1041 Bouchet, B.P., Grigoriev, I., Spangler, S.A., Yu, K.L., et al. (2013). CFEOM1-Associated
1042 Kinesin KIF21A Is a Cortical Microtubule Growth Inhibitor. Developmental Cell *27*, 145–160.
1043 10.1016/j.devcel.2013.09.010.

1044 23. Shin, H., Wyszynski, M., Huh, K.-H., Valtschanoff, J.G., Lee, J.-R., Ko, J., Streuli, M.,
1045 Weinberg, R.J., Sheng, M., and Kim, E. (2003). Association of the Kinesin Motor KIF1A with
1046 the Multimodular Protein Liprin-α. Journal of Biological Chemistry *278*, 11393–11401.
1047 10.1074/jbc.M211874200.

1048 24. Spangler, S.A., Jaarsma, D., De Graaff, E., Wulf, P.S., Akhmanova, A., and Hoogenraad,
1049 C.C. (2011). Differential expression of liprin-α family proteins in the brain suggests
1050 functional diversification. J. Comp. Neurol. *519*, 3040–3060. 10.1002/cne.22665.

1051 25. Zürner, M., and Schoch, S. (2009). The mouse and human Liprin-α family of scaffolding
1052 proteins: Genomic organization, expression profiling and regulation by alternative splicing.
1053 Genomics *93*, 243–253. 10.1016/j.ygeno.2008.10.007.

1054 26. Zürner, M., Mittelstaedt, T., tom Dieck, S., Becker, A., and Schoch, S. (2011). Analyses of
1055 the spatiotemporal expression and subcellular localization of liprin-α proteins. J. Comp.
1056 Neurol. *519*, 3019–3039. 10.1002/cne.22664.

1057 27. Wong, M.Y., Liu, C., Wang, S.S.H., Roquas, A.C.F., Fowler, S.C., and Kaeser, P.S. (2018).
1058 Liprin-α3 controls vesicle docking and exocytosis at the active zone of hippocampal
1059 synapses. Proc. Natl. Acad. Sci. U.S.A. *115*, 2234–2239. 10.1073/pnas.1719012115.

1060 28. Kang, H.J., Kawasawa, Y.I., Cheng, F., Zhu, Y., Xu, X., Li, M., Sousa, A.M.M., Pletikos, M.,
1061 Meyer, K.A., Sedmak, G., et al. (2011). Spatio-temporal transcriptome of the human brain.
1062 Nature *478*, 483–489. 10.1038/nature10523.

1063 29. Zhen, M., and Jin, Y. (1999). The liprin protein SYD-2 regulates the differentiation of
1064 presynaptic termini in C. elegans. Nature *401*, 371–375. 10.1038/43886.

1065 30. Kittelmann, M., Hegermann, J., Goncharov, A., Taru, H., Ellisman, M.H., Richmond, J.E.,
1066 Jin, Y., and Eimer, S. (2013). Liprin-α/SYD-2 determines the size of dense projections in
1067 presynaptic active zones in C. elegans. Journal of Cell Biology *203*, 849–863.
1068 10.1083/jcb.201302022.

1069 31. Patel, M.R., and Shen, K. (2009). RSY-1 Is a Local Inhibitor of Presynaptic Assembly in *C.*
1070 *elegans*. Science *323*, 1500–1503. 10.1126/science.1169025.

1071 32. Kaufmann, N., DeProto, J., Ranjan, R., Wan, H., and Van Vactor, D. (2002). Drosophila
1072 Liprin-α and the Receptor Phosphatase Dlar Control Synapse Morphogenesis. Neuron *34*,
1073 27–38. 10.1016/S0896-6273(02)00643-8.

1074 33. Astigarraga, S., Hofmeyer, K., Farajian, R., and Treisman, J.E. (2010). Three *Drosophila*
1075 Liprins Interact to Control Synapse Formation. J. Neurosci. *30*, 15358–15368.
1076 10.1523/JNEUROSCI.1862-10.2010.

1077 34. Hofmeyer, K., Maurel-Zaffran, C., Sink, H., and Treisman, J.E. (2006). Liprin-α has LAR-
1078 independent functions in R7 photoreceptor axon targeting. Proc. Natl. Acad. Sci. U.S.A.
1079 *103*, 11595–11600. 10.1073/pnas.0604766103.

1080 35. Amberger, J., Bocchini, C.A., Scott, A.F., and Hamosh, A. (2009). McKusick's Online
1081 Mendelian Inheritance in Man (OMIM). Nucleic Acids Res *37*, D793-796.
1082 10.1093/nar/gkn665.

1083 36. Samocha, K.E., Robinson, E.B., Sanders, S.J., Stevens, C., Sabo, A., McGrath, L.M.,
1084 Kosmicki, J.A., Rehnström, K., Mallick, S., Kirby, A., et al. (2014). A framework for the
1085 interpretation of de novo mutation in human disease. Nat Genet *46*, 944–950.
1086 10.1038/ng.3050.

1087 37. Karczewski, K.J., Francioli, L.C., Tiao, G., Cummings, B.B., Alföldi, J., Wang, Q., Collins,
1088 R.L., Laricchia, K.M., Ganna, A., Birnbaum, D.P., et al. (2020). The mutational constraint
1089 spectrum quantified from variation in 141,456 humans. Nature *581*, 434–443.
1090 10.1038/s41586-020-2308-7.

1091 38. Arachchi, H., Wojcik, M.H., Weisburd, B., Jacobsen, J.O.B., Valkanas, E., Baxter, S., Byrne,
1092 A.B., O'Donnell-Luria, A.H., Haendel, M., Smedley, D., et al. (2018). *matchbox* : An open-

1093 source tool for patient matching via the Matchmaker Exchange. Human Mutation *39*, 1827–
1094 1834. 10.1002/humu.23655.

1095 39. Sobreira, N., Schiettecatte, F., Valle, D., and Hamosh, A. (2015). GeneMatcher: A Matching
1096 Tool for Connecting Investigators with an Interest in the Same Gene. Human Mutation *36*,
1097 928–930. 10.1002/humu.22844.

1098 40. Philippakis, A.A., Azzariti, D.R., Beltran, S., Brookes, A.J., Brownstein, C.A., Brudno, M.,
1099 Brunner, H.G., Buske, O.J., Carey, K., Doll, C., et al. (2015). The Matchmaker Exchange: A
1100 Platform for Rare Disease Gene Discovery. Human Mutation *36*, 915–921.
1101 10.1002/humu.22858.

1102 41. Chao, H.-T., Davids, M., Burke, E., Pappas, J.G., Rosenfeld, J.A., McCarty, A.J., Davis, T.,
1103 Wolfe, L., Toro, C., Tifft, C., et al. (2017). A Syndromic Neurodevelopmental Disorder
1104 Caused by De Novo Variants in EBF3. The American Journal of Human Genetics *100*, 128–
1105 137. 10.1016/j.ajhg.2016.11.018.

1106 42. Bischof, J., Sheils, E.M., Björklund, M., and Basler, K. (2014). Generation of a transgenic
1107 ORFeome library in Drosophila. Nat Protoc *9*, 1607–1620. 10.1038/nprot.2014.105.

1108 43. Gahl, W.A., Mulvihill, J.J., Toro, C., Markello, T.C., Wise, A.L., Ramoni, R.B., Adams, D.R.,
1109 and Tifft, C.J. (2016). The NIH Undiagnosed Diseases Program and Network: Applications
1110 to modern medicine. Molecular Genetics and Metabolism *117*, 393–400.
1111 10.1016/j.ymgme.2016.01.007.

1112 44. Kircher, M., Witten, D.M., Jain, P., O'Roak, B.J., Cooper, G.M., and Shendure, J. (2014). A
1113 general framework for estimating the relative pathogenicity of human genetic variants.
1114 Nature Genetics *46*, 310–315. 10.1038/ng.2892.

1115 45. Menon, K.P., Carrillo, R.A., and Zinn, K. (2013). Development and plasticity of the
1116 *Drosophila* larval neuromuscular junction: Development and plasticity of the neuromuscular
1117 junction. WIREs Dev Biol *2*, 647–670. 10.1002/wdev.108.

1118 46. Collins, C.A., and DiAntonio, A. (2007). Synaptic development: insights from Drosophila.
1119 Current Opinion in Neurobiology *17*, 35–42. 10.1016/j.conb.2007.01.001.

1120 47. Green, J.B., Gardner, C.D., Wharton, R.P., and Aggarwal, A.K. (2003). RNA Recognition via
1121 the SAM Domain of Smaug. Molecular Cell *11*, 1537–1548. 10.1016/S1097-2765(03)00178-
1122 3.

1123 48. Barrera, F.N., Poveda, J.A., González-Ros, J.M., and Neira, J.L. (2003). Binding of the C-
1124 terminal Sterile α Motif (SAM) Domain of Human p73 to Lipid Membranes. Journal of
1125 Biological Chemistry *278*, 46878–46885. 10.1074/jbc.M307846200.

1126 49. Kaufmann, N., DeProto, J., Ranjan, R., Wan, H., and Van Vactor, D. (2002). Drosophila
1127 Liprin-α and the Receptor Phosphatase Dlar Control Synapse Morphogenesis. Neuron *34*,
1128 27–38. 10.1016/S0896-6273(02)00643-8.

1129 50. MacDonald, J.R., Ziman, R., Yuen, R.K.C., Feuk, L., and Scherer, S.W. (2014). The
1130 Database of Genomic Variants: a curated collection of structural variation in the human
1131 genome. Nucleic Acids Res *42*, D986-992. 10.1093/nar/gkt958.

51. Landrum, M.J., Lee, J.M., Benson, M., Brown, G.R., Chao, C., Chitipiralla, S., Gu, B., Hart, J., Hoffman, D., Jang, W., et al. (2018). ClinVar: improving access to variant interpretations and supporting evidence. Nucleic Acids Res *46*, D1062–D1067. 10.1093/nar/gkx1153.

178
179 Table 1: Genetic and Neurologic findings in individuals with rare *PPFIA3* variants and neurodevelopmental disorders

Individual	1	2	3	4	5	6	7	8	9	10
Family	F1	F2	F3	F4	F5	F5	F6	F7	F8	F9
cDNA (NM_003660.4)	c.115 C>T	c.115 C>T	c.118 G>A	c.239 A>C	c.240+1 G>A	c.240+1 G>A	c.943 G>T	c.1243 C>T	c.1243 C>T	c.1285 C>T
Protein (NP_003651.1)	p.(Arg39Cys)	p.(Arg39Cys)	p.(Glu40Lys)	p.(Gln80Pro)	n/a	n/a	p.(Ala315Ser)	p.(Arg415Trp)	p.(Arg415Trp)	p.(Arg429Trp)
Human reference genome	GRCh37 (hg19)	GRCh37 (hg19)	GRCh37 (hg19)	GRCh37 (hg19)	GRCh37 (hg19)	GRCh37 (hg19)	GRCh37 (hg19)	GRCh37 (hg19)	GRCh37 (hg19)	GRCh37 (hg19)
Variant inheritance	de novo	de novo	not from mother; father unavailable for testing	unknown	inherited from affected mother (individual 6)	unknown	de novo	de novo	unknown	de novo
gnomAD (v2.1.1)	not present	not present	not present	not present	not present	not present	not present	not present	not present	not present
Mosaicism	no	no	no	no	no	no	no	no	no	yes
Sex	male	male	female	female	female	female	female	female	female	female
Age at most recent assessment	16 years	13 years	22 years	1 year and 10 months	5 years	35 years	neonatal	8 years	10 years 9 months	n/a
Racial and Ethnic Categories (NIH)	White	family declined to answer	White	White	White	White	Latino	Mixed European and Asian	Asian	White
Status	alive	alive	alive	alive	alive	alive	deceased	alive	alive	elective pregnancy termination
Abnormal EEG	yes	yes	yes	n/a	n/a	n/a	n/a	yes	yes	n/a
Epilepsy	yes	yes	yes	no	no	no	n/a	yes	n/a	n/a
Autism or autistic features	no	no	no	suspected	no	n/a	n/a	autistic features	autistic features	n/a
Dysmorphisms	yes	yes	yes	yes	yes	yes	yes	yes	yes	n/a

180
181 Abbreviations: electroencephalogram (EEG), no information available (n/a)
182

183

Individual	11	12	13	14	15	16	17	18	19	20
Family	F10	F11	F12	F13	F13	F14	F15	F16	F17	F18
cDNA (NM_003660.4)	c.1492 C>T	c.1638 G>T	c.2350 C>T	c.2609 T>A	c.2609 T>A	c.2706dup	c.2717 C>T	c.3307del	deletion exons 22-30	c.[2377C>A]; [c.2276 A>G]
Protein (NP_003651.1)	p.(Arg498Trp)	p.(Trp546Cys)	p.(Arg784Trp)	p.(Ile870Asn)	p.(Ile870Asn)	p.(Ser903Leu fs*86)	p.(Ser906Leu)	p.(Glu1103Asnfs*8)	n/a	p.[Pro793Thr]; p.[Lys759Arg]
Human reference genome	GRCh37 (hg19)	GRCh37 (hg19)	GRCh37 (hg19)	GRCh37 (hg19)	GRCh37 (hg19)	GRCh37 (hg19)	GRCh37 (hg19)	GRCh37 (hg19)	GRCh38 (hg38)	GRCh37 (hg19)
Variant inheritance	de novo	de novo	de novo	de novo (monozygotic twin of individual 15)	de novo (monozygotic twin of individual 14)	unknown	de novo	unknown	inherited, affected mother	inherited from unaffected mother and father
gnomAD (v2.1.1)	not present	not present	frequency of 3.19×10^{-5} (1/31,386)	not present	not present	not present	not present	not present	n/a	p.(Pro793Thr) frequency of 7.61×10^{-4} (215/282,366); p.(Lys759Arg) frequency of 4.77x10-5 (13/282,880)
Mosaicism	no	no	no	no	no	n/a	no	no	n/a	none
Sex	male	male	female	female	female	male	female	female	male	male
Age at most recent assessment	6 years 11 months	11 years	16 years	5 years	5 years	23 years	13 years 11 months	9 years 9 months	7 years 8 months	9 years
Racial and Ethnic Categories (NIH)	Asian	White	White	White	White	White	White	White	White	White
Status	alive	alive	alive	alive	alive	alive	alive	alive	alive	alive
Abnormal EEG	n/a	no	yes	n/a	n/a	n/a	yes	yes	no	yes
Epilepsy	no	no	yes	no	no	n/a	no	no	no	yes
Autism or autistic features	yes, autistic features improved over last few years	yes	no	yes	no	autistic features	yes	no	n/a	autistic features
Dysmorphisms	Yes	no	no	no	no	n/a	Yes	Yes	Yes	Yes

184

185 Table 2: In silico predictions for *PPFIA3* variants
186

Individuals	1 and 2	3	4	5 and 6	7	8 and 9	10	11
Human reference genome	GRCh37 (hg19)	GRCh37 (hg19)	GRCh37 (hg19)	GRCh37 (hg19)	GRCh37 (hg19)	GRCh37 (hg19)	GRCh37 (hg19)	GRCh37 (hg19)
PPFIA3 variant cDNA (NM_003660.4:)	c.115 C>T	c.118G>A	c.239 A>C	c.240+1G>A	c.943 G>T	c.1243 C>T	c.1285 C>T	c.1492 C>T
PPFIA3 variant protein (NP_003651.1:)	p.(Arg39Cys)	p.(Glu40Lys)	p.(Gln80Pro)	n/a	p.(Ala315Ser)	p.(Arg415Trp)	p.(Arg429Trp)	p.(Arg498Trp)
REVEL (v1)	0.316	0.271	0.338	n/a	0.218	0.21	0.295	0.273
CADD (v1.6)	31	30	26.8	34	24	33	29.2	25.9
GERP	4.19	4.19	4.34	4.34	4.29	2.12	2.95	1.41
M-CAP (v1.4)	Possibly Pathogenic	Possibly Pathogenic	Possibly Pathogenic	n/a	Possibly Pathogenic	Likely Benign	Possibly Pathogenic	Possibly Pathogenic
PolyPhen2 HumDiv	Probably damaging	Probably Damaging	Benign	n/a	Benign	Probably Damaging	Probably damaging	Probably damaging
PolyPhen2 HumVar	Probably damaging	Probably Damaging	Benign	n/a	Benign	Probably Damaging	Probably damaging	Probably damaging
Phylop Vertebrate	0.945	9.447	9.02	n/a	9.4308	0.0498	2.25	2.58
SIFT	Damaging	Damaging	Damaging	n/a	Damaging	Damaging	Damaging	Damaging

187
188
189
190
191
192
193

194
195 Abbreviations: combined annotation dependent depletion (CADD); genomic evolutionary rate profiling (GERP); Mendelian clinically applicable pathogenicity (M-CAP); polymorphism phenotyping v2

Individuals	12	13	14 and 15	16	17	18	19	20	20
Human reference genome	GRCh37 (hg19)	GRCh37 (hg19)	GRCh37 (hg19)	GRCh37 (hg19)	GRCh37 (hg19)	GRCh37 (hg19)	GRCh38 (hg38)	GRCh37 (hg19)	GRCh37 (hg19)
PPFIA3 variant cDNA (NM_003660.4:)	c.1638 G>T	c.2350 C>T	c.2609 T>A	c.2706dup	c.2717 C>T	c.3307del	deletion exons 22-30[a]	c.2377C>A	c.2276 A>G
PPFIA3 variant protein (NP_003651.1:)	p.(Trp546Cys)	p.(Arg784Trp)	p.(Ile870Asn)	p.Ser903Leu fs*86)	p.(Ser906Leu)	p.(Glu1103Asnfs*8)	n/a	p.(Pro793Thr)	p.(Lys759Arg)
REVEL (v1)	0.186	0.158	0.41	n/a	0.207	n/a	n/a	0.092	0.183
CADD (v1.6)	25.6	26.5	31	n/a	29.3	54	49	22.6	26.8
GERP	3.87	3.63	4.45	4.45	3.31	4.29	n/a	4.91	4.17
M-CAP (v1.4)	Possibly Pathogenic	Possibly Pathogenic	Possibly Pathogenic	n/a	Likely Benign	n/a	n/a	Possibly pathogenic	Possibly pathogenic
PolyPhen2 HumDiv	Probably damaging	Probably damaging	Probably damaging	n/a	Tolerated	n/a	n/a	Probably damaging	Probably damaging
PolyPhen2 HumVar	Probably damaging	Benign	Probably damaging	n/a	Probably damaging	n/a	n/a	Probably damaging	Probably damaging
Phylop Vertebrate	4	1.609	7.855	n/a	5.756	n/a	n/a	3.7	9.17
SIFT	Tolerated	Damaging	Damaging	n/a	Damaging	n/a	n/a	Damaging	Damaging

196 (PolyPhen2); sorting intolerant from tolerant (SIFT); not applicable (n/a); [a]no further information is available for the breakpoints for deletion in Individual 19.
197
198
199
200
201
202
203
204
205
206
207
208
209
210
211

Table 3: Comparison of clinical phenotypes and findings in fruit flies expressing *PPFIA3* missense variants

236
237 Abbreviations: electroencephalogram (EEG), delayed development (DD), intellectual disability (ID), no information available (n/a), loss of function (LOF), neuromuscular junction (NMJ), not available (n/a)

	PPFIA3 variants (GRCh37, hg19)	c.115 C>T (p.Arg39Cys)		c.943 G>T (p.Ala315Ser)	c.1243 C>T (p.Arg415Trp)		c.1638 G>T (p.Trp546Cys)	c.2350 C>T (p.Arg784Trp)
	Individual	1	2	7	8	9	12	13
Key clinical phenotypes in individuals with *PPFIA3* variants	Location	Coiled-coil		Coiled-coil	Coiled-coil		Disordered region	Disordered region
	Abnormal EEG	+	+	n/a	+	+	-	+
	Epilepsy	+	-	n/a	+	-	-	+
	Autism/autistic features	-	-	n/a	+	+	+	-
	DD/ID	+	+	n/a	+	+	+	+
	Hypotonia	+	n/a	n/a	+	-	-	-
	Dysmorphisms	+	+	+	+	n/a	-	-
	Micro- or macrocephaly	-	-	+	+	n/a	-	-
	Clinical features (# present / total reported)	5/7	3/6	2/2	7/7	3/5	2/7	3/7
Findings in fruit flies expressing *PPFIA3* variants	Eclosion defect	+	+	+	-	-	-	+
	Abnormal leg morphology	+	+	+	-	-	-	+
	Climbing defect	+	+	+	-	+	-	+
	Bang sensitivity	+	+	+	-	-	-	+
	NMJ defect	+	n/a	+	-	-	-	+
	Liprin-α LOF rescue defect	+	n/a	+	-	+	-	+
	Fly phenotypes (# present / total assays)	6/6	4/4	6/6	0/6	2/6	0/6	6/6
	Variant severity according to the number of phenotypes in fly assays (0: no effect in fly assays; 1-2 mild; 3-4 moderate; 5-6 severe)	severe	at least moderate	severe	no effect	mild	no effect	severe

238
239

Figure 1

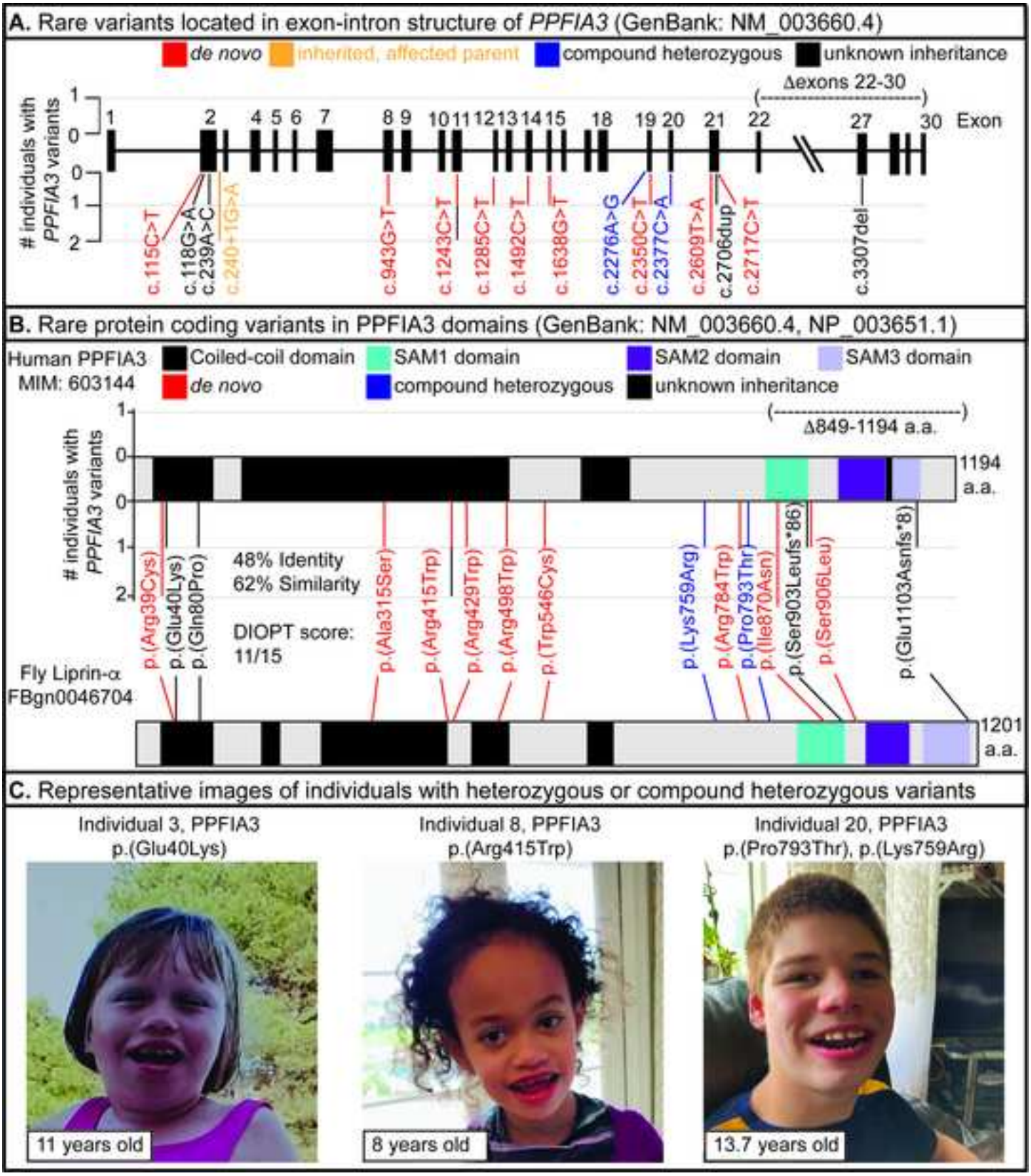

Figure 2

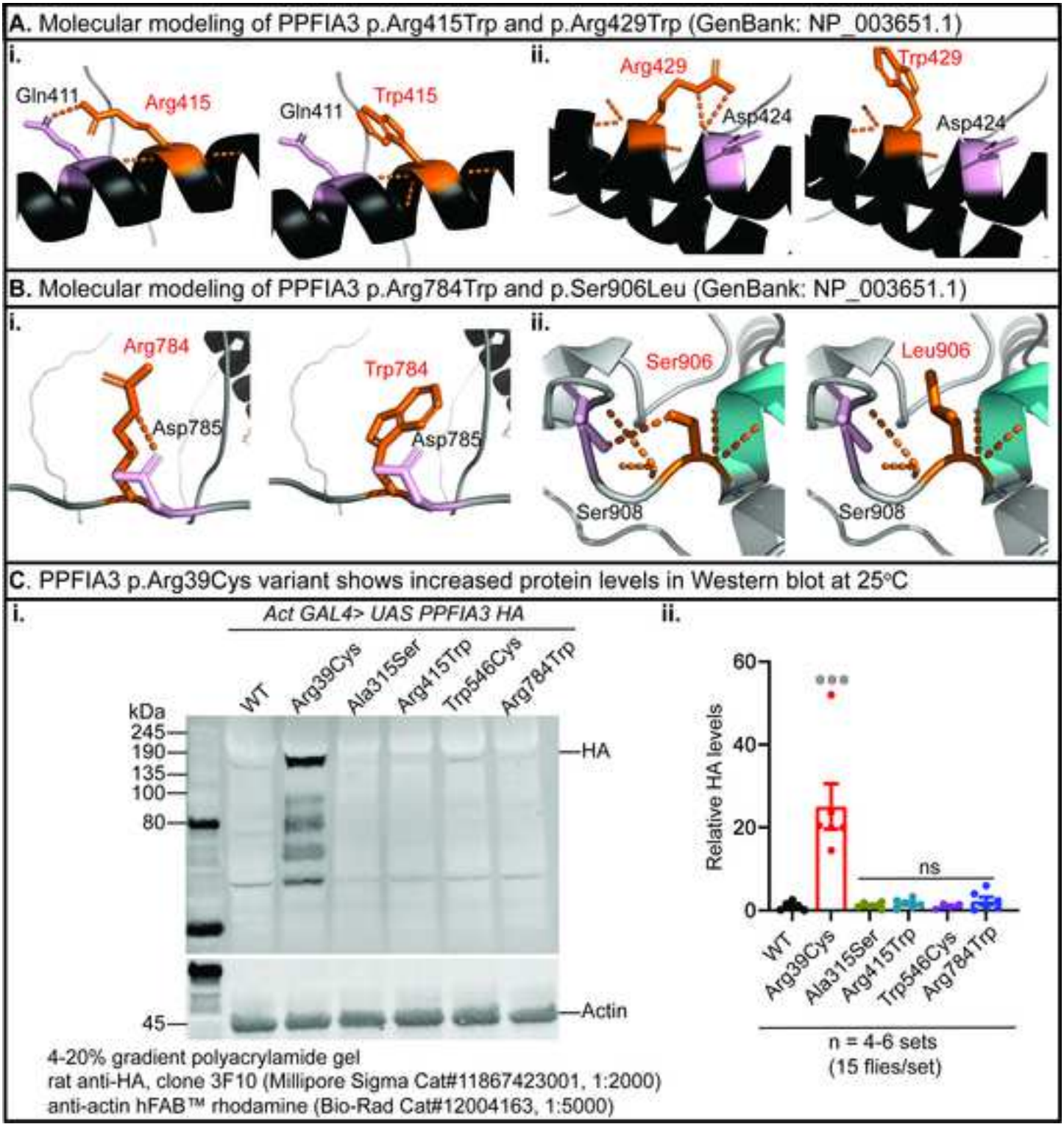

Figure 3

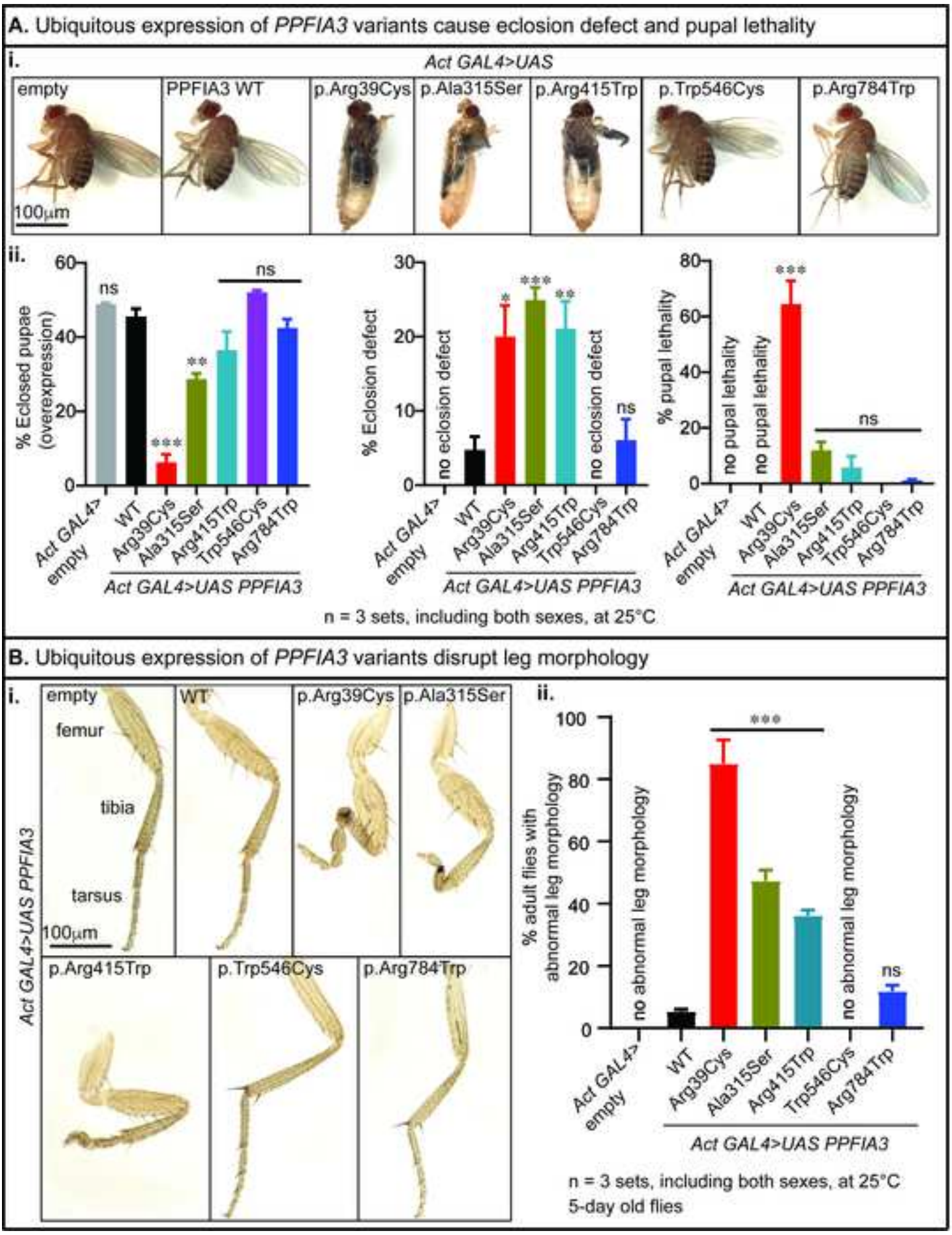

Figure 4

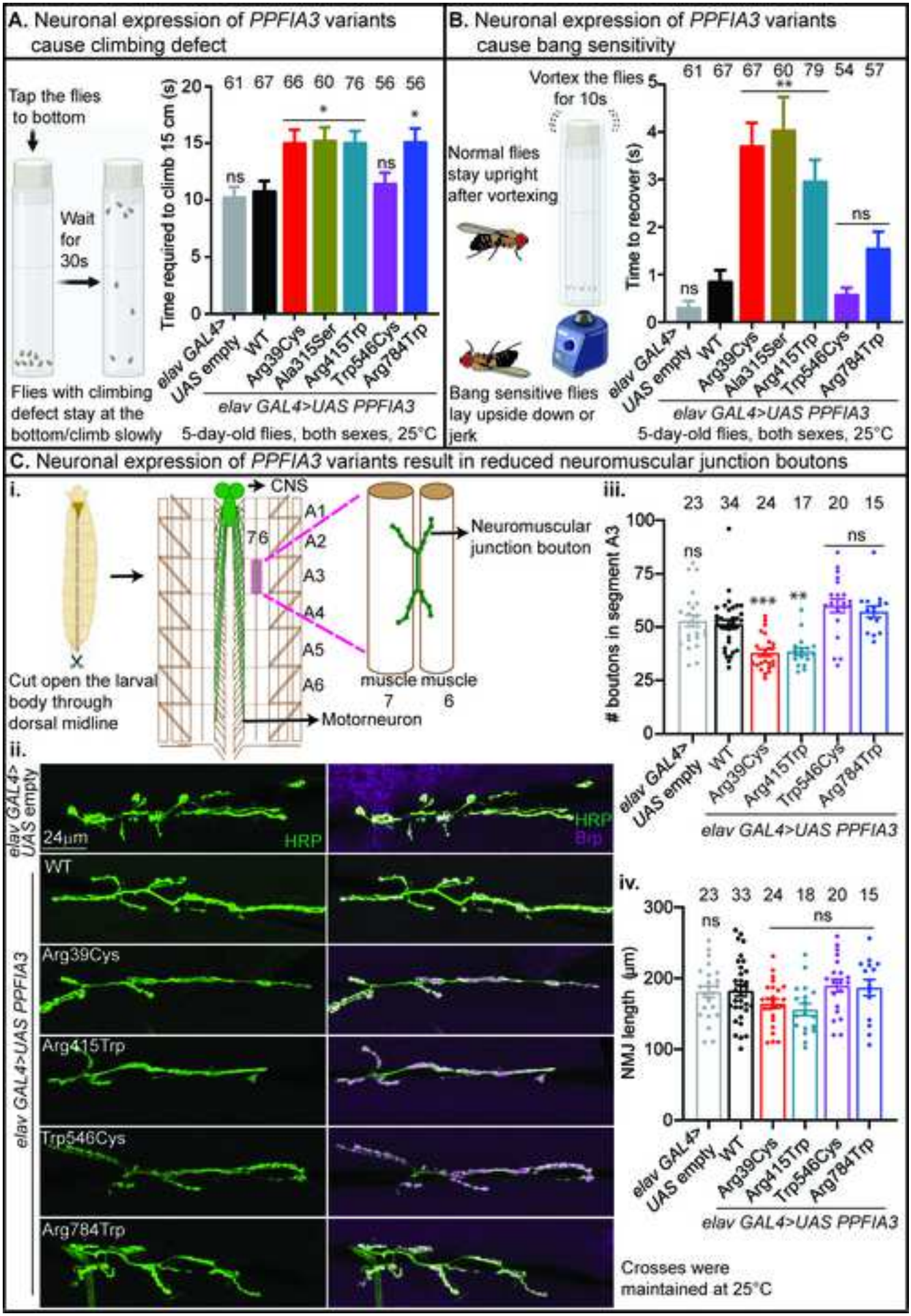

Figure 5

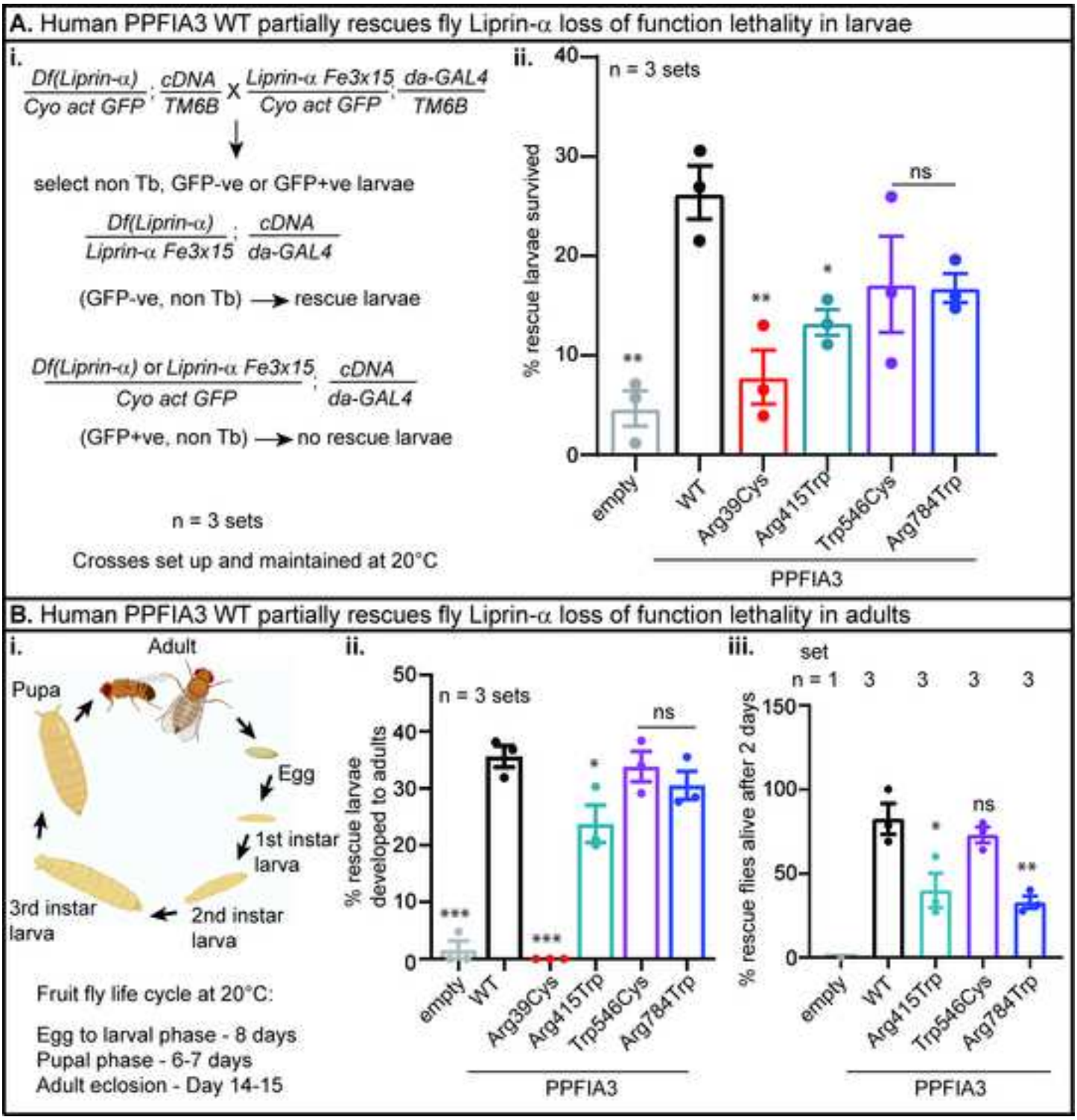

Table S3

Click here to access/download

Supplemental Movies and Spreadsheets

Table S3_Stat Summary_2023-10-26_draft 5_MP.xlsx

Table S4

Click here to access/download

Supplemental Movies and Spreadsheets

Table S4_1to10_Gen info&clini find_2023-11-28_d11_HTC.xlsx

Table S5

Click here to access/download

Supplemental Movies and Spreadsheets

Table S5_11to20_Gen info&clin finds_2023-11-30_rev v10_HTC.xlsx

Table S6

Click here to access/download

Supplemental Movies and Spreadsheets

Table S6_ Dev milestones_2023-11-22_draft7_HTC.xlsx

Table S8

Click here to access/download

Supplemental Movies and Spreadsheets

Table S8_PPFIA3 CNV_2023-11-28_draft 7_MP.xlsx

eTOC blurb

PPFIA3 is a scaffolding protein that mediates synaptic transmission. This study identified 20 individuals with *PPFIA3* variants associated with developmental delay, intellectual disability, hypotonia, dysmorphisms, micro/macrocephaly, autistic features, and epilepsy. Functional analysis shows that PPFIA3 variants cause a syndromic neurodevelopmental disorder through a potential loss of function mechanism.